
SPARSE ADDITIVE GAUSSIAN PROCESS REGRESSION

A PREPRINT

Hengrui Luo
 Department of Statistics
 The Ohio State University
 Columbus, OH 43210, USA
 luo.619@osu.edu

Giovanni Nattino
 Division of Biostatistics, College of Public Health
 The Ohio State University
 Columbus, OH 43210, USA
 nattino.1@osu.edu

Matthew T. Pratola
 Department of Statistics
 The Ohio State University
 Columbus, OH 43210, USA
 mpratola@stat.osu.edu

March 25, 2022

ABSTRACT

In this paper we introduce a novel model for Gaussian process (GP) regression in the fully Bayesian setting. Motivated by the idea of sparsification, localization and Bayesian additive modeling, our model is built around a recursive partitioning (RP) scheme. Within each RP partition, a sparse GP regression model is fitted. A Bayesian additive framework combines the partitions, allowing the model to admit both global trends and local refinements on which a sparse GP construction enables efficient computation. The model addresses both the problem of efficiency in fitting a full Gaussian process regression model and the problem of prediction performance associated with a single sparse Gaussian process. Our approach mitigates the issue of pseudo-input selection and avoids the need for complex inter-block correlations in existing approaches. Furthermore, the proposed model can also capture non-stationarity. The crucial trade-off becomes choosing between many simpler local model components or fewer complex global model components, which can be easily and sensibly tuned by the practitioner. Implementation is via a straightforward Metropolis-Hasting Markov chain Monte-Carlo algorithm. We compare our model against popular alternatives with simulated and real datasets, and find the performance is competitive, while the fully Bayesian procedure enables the quantification of model uncertainties.

Keywords Sparse Gaussian Process · Recursive Partition Scheme · Bayesian Additive Model · Nonparametric Regression

1 Introduction

Gaussian process (GP) regression is widely adopted for fitting a variety of data, especially non-stationary and nonlinear data [Rasmussen and Williams, 2006]. Taking a Bayesian GP modeling approach, the posterior provides a natural uncertainty quantification, and more generally Bayesian inference provides nice theoretical properties [Gelman et al., 2013]. However, the computational cost for likelihood evaluations based on an observed dataset $\{y, \mathcal{X}\}$ of size n is of order $\mathcal{O}(n^3)$, which primarily results from the need to invert an $n \times n$ covariance matrix. Therefore, the computational cost could be prohibitively high in scenarios where large datasets need to be analyzed.

It is a focus of much current research to solve this problem of high computational cost for GP regression [Banerjee et al., 2012, Liu et al., 2018]. There are multiple approaches to circumvent this problem, such as low-rank covariance approximation [Rasmussen and Williams, 2006], model likelihood approximations [Kaufman et al., 2008] and local GP approximations [Snelson and Ghahramani, 2007, Gramacy and Apley, 2015]. For a comprehensive review of approximation methods in GP modeling, we refer the interested reader to Liu et al. [2018].

Another research interest in GP regression, primarily in spatial statistics, concerns how to model non-stationary data [Paciorek and Schervish, 2004, 2006]. It is known that GP regression cannot handle non-stationarity when using classical covariance kernels. One popular method of modeling non-stationary datasets is to use localization approaches [Gramacy and Apley, 2015, Park and Huang, 2016]. The idea of localization is to subset the data into local sub-regions of the input domain and then fit stationary GP regressions independently in each region, leading to a globally non-stationary model.

To alleviate the computational problem and address non-stationarity, we are inspired by the idea of sparsification [Snelson and Ghahramani, 2006, Titsias, 2009a] and the widely used localization method of partition schemes [Chipman et al., 1998, Roy and Teh, 2008, Nguyen-Tuong et al., 2009, Gramacy and Apley, 2015, Chipman et al., 2016, Lee et al., 2017]. Under the framework of Bayesian (generalized) additive modeling [Hastie and Tibshirani, 1990, 2000], we attempt to combine the advantages of these two approaches to reduce or eliminate the computational constraint by using partition blocks as additive components.

In this work we propose a novel approach, the Sparse Additive Gaussian Process (SAGP) model, that combines the sparse GP approximation with a recursive partition (RP) scheme while preserving a full Bayesian framework. It turns out that our approach can handle both local and global features simultaneously in large datasets while realizing large gains in computational efficiency. Not only does it provide natural uncertainty quantification for parameters and predictions from posterior samples, but also has the advantage of learning the inter-block correlation from the model.

Instead of using a more computationally involved dynamic partition scheme (e.g. Chipman et al. 1998, 2016), we propose a simpler static recursive scheme. We will see later that this simpler scheme brings convenience in algorithmic design, interpretation and trade-offs between sparsity and number of partitions. SAGP modeling is flexible in the sense that not only does it have the advantage of capturing multi-scale features, but also attains high computational efficiency using both the idea of sparsification and the idea of localization. To our best knowledge, this kind of intuitively attractive Bayesian model combining these ideas has not been investigated previously.

The organization of the paper will be as follows. In section 2 we will briefly review the background knowledge for sparse GP, localization and Bayesian additive modeling as they are essential ingredients of SAGP modeling. In section 3 we will specify the SAGP model. Sections 4 and 5 are analysis and comparison based on simulated and real-world datasets respectively. Finally, we conclude our paper with a discussion in section 6.

2 Background

2.1 Gaussian Process Regression

We start with GP regression and use the notation $N_d(\mathbf{m}, \Sigma)$ to denote the d -dimensional Gaussian distribution with mean vector \mathbf{m} and covariance matrix Σ and the notation $N_d(\mathbf{y} | \mathbf{m}, \Sigma)$ to denote the d -dimensional Normal density evaluated at $\mathbf{y} \in \mathbb{R}^n$. The prior of the mean regression function is assumed to be a GP with known mean and covariance kernel function. The posterior estimation and prediction from the regression model is from combining this prior and the information contained in the likelihood of response variables $\mathbf{y} = (y_1, \dots, y_n)^T$ observed at known input locations $\mathcal{X} = \{\mathbf{x}_i \in \mathbb{R}^d, i = 1, \dots, n\}$ using Bayes theorem. The general regression problem is to estimate an unknown mean function $f(\mathbf{x}) : \mathbb{R}^d \rightarrow \mathbb{R}$, given the observations \mathbf{y} . We also call f the target and the variable \mathbf{x}_i the input, based on the model form

$$\begin{aligned} y(\mathbf{x}_i) &= f(\mathbf{x}_i) + \epsilon_i, i = 1, \dots, n \\ \epsilon_i &\sim N_1(0, \sigma_\epsilon^2) \end{aligned} \quad (1)$$

which expresses the relationship between input \mathbf{x}_i and the unknown response $f(\mathbf{x}_i)$ observed as y_i with observational error ϵ_i having the variance $\sigma_\epsilon^2 > 0$. Using vector notations we can write $\mathbf{y} = (y_1, \dots, y_n)^T = (y(\mathbf{x}_1), y(\mathbf{x}_2), \dots, y(\mathbf{x}_n))^T$, $\mathbf{f} = (f(\mathbf{x}_1), \dots, f(\mathbf{x}_n))^T$ and the noise $\boldsymbol{\epsilon} \sim N_n(\mathbf{0}_n, \sigma_\epsilon^2 \mathbf{I}_n)$ to yield

$$\mathbf{y} = \mathbf{f} + \boldsymbol{\epsilon}. \quad (2)$$

In addition, with appropriate scaling and normalization if needed, GP regression (2) assumes that the mean vector \mathbf{f} is a realization of a zero mean Gaussian process, $\mathbf{f} \sim N_n(\mathbf{0}, \mathbf{K}_n)$, where $\mathbf{K}_n = [K(\mathbf{x}_i, \mathbf{x}_j)]_{i,j=1}^n$, with covariance kernel $K(\cdot, \cdot) : \mathbb{R}^d \times \mathbb{R}^d \rightarrow \mathbb{R}$ encoding assumed properties of the unknown function f to satisfy the application of interest [Rasmussen and Williams, 2006].

2.2 Sparsification of Gaussian Processes

One popular kind of sparse covariance matrix approximation is the pseudo-input (or latent variable) approach. This approach is also known as the Sparse Gaussian Process (SGP). By replacing the exact covariance matrix in the likelihood computation with an approximation, one can greatly reduce computational cost. There are various sparse approximation approaches (e.g. Lawrence et al. 2003, Quinonero-Candela and Rasmussen 2005). In this paper we follow the idea of Snelson and Ghahramani [2006], who use a subset of the full inputs $\mathcal{X} = \{\mathbf{x}_1, \dots, \mathbf{x}_n\}$ as pseudo-inputs, denoted as $\bar{\mathcal{X}} = \{\bar{\mathbf{x}}_1, \dots, \bar{\mathbf{x}}_m\}$, for $m \ll n$, and the notation $\bar{\mathbf{f}} = (f(\bar{\mathbf{x}}_1), f(\bar{\mathbf{x}}_2), \dots, f(\bar{\mathbf{x}}_m))^T$ as the vector of pseudo-targets.

The notations

$$\begin{aligned} \mathbf{K}_n &:= [K(\mathbf{x}_k, \mathbf{x}_l)]_{k,l=1}^n, \\ \mathbf{K}_m &:= [K(\bar{\mathbf{x}}_k, \bar{\mathbf{x}}_l)]_{k,l=1}^m, \\ \mathbf{K}_{nm} &= [K(\mathbf{x}_i, \bar{\mathbf{x}}_j)]_{i,j=1}^{n,m} = \mathbf{K}_{mn}^T \end{aligned}$$

denote the (cross-)covariance matrix between full targets \mathbf{f} and pseudo-targets $\bar{\mathbf{f}}$. It relates the full covariance matrix and the sparse approximating covariance matrix conditioned on the pseudo-inputs and parameters. The posterior as well as predictive posterior can be written in closed form by Gaussian conjugacy as shown in Snelson and Ghahramani [2006]. For an SGP model with m pseudo-inputs, the full likelihood is $P(\mathbf{y} \mid \mathcal{X}, \bar{\mathcal{X}}, \bar{\mathbf{f}}) = N_n(\mathbf{y} \mid \mathbf{K}_{nm} \mathbf{K}_m^{-1} \bar{\mathbf{f}}, \Lambda + \sigma_\epsilon^2 \mathbf{I}_n)$ where $\Lambda = \text{diag} \left(K(\mathbf{x}_i, \mathbf{x}_i) - \mathbf{k}_i^T \mathbf{K}_m^{-1} \mathbf{k}_i \right)_{i=1}^n$. The posterior distribution over pseudo-targets is $P(\bar{\mathbf{f}} \mid \mathcal{X}, \mathbf{y}, \bar{\mathcal{X}}) = N_m(\bar{\mathbf{f}} \mid \mathbf{K}_m \mathbf{Q}_m^{-1} \mathbf{K}_{mn} (\Lambda + \sigma_\epsilon^2 \mathbf{I})^{-1} \mathbf{y}, \mathbf{K}_m \mathbf{Q}_m^{-1} \mathbf{K}_m)$ where $\mathbf{Q}_m = \mathbf{K}_m + \mathbf{K}_{mn} (\Lambda + \sigma_\epsilon^2 \mathbf{I})^{-1} \mathbf{K}_{nm}$. Here we follow the notation convention that $\mathbf{k}_i = (K(\bar{\mathbf{x}}_1, \mathbf{x}_i), \dots, K(\bar{\mathbf{x}}_m, \mathbf{x}_i))^T$. The predictive posterior distribution for y^* at a new location \mathbf{x}^* , after integrating out the pseudo-target $\bar{\mathbf{f}}$, can be written as $P(y^* \mid \mathbf{x}_*, \mathcal{X}, \mathbf{y}, \bar{\mathcal{X}}) = N_1(\mathbf{k}_*^T \mathbf{Q}_m^{-1} \mathbf{K}_{mn} (\Lambda_n + \sigma_\epsilon^2 \mathbf{I}_n)^{-1} \mathbf{y}, \sigma_\epsilon^2 + K_{**} - \mathbf{k}_*^T \mathbf{K}_m^{-1} \mathbf{k}_* + \mathbf{k}_*^T \mathbf{Q}_m^{-1} \mathbf{k}_*)$, where $\mathbf{k}_* = (K(\bar{\mathbf{x}}_1, \mathbf{x}_*), \dots, K(\bar{\mathbf{x}}_m, \mathbf{x}_*))^T$. It is not hard to see that when $n = m$ we obtain the posterior distributions of the full Gaussian process model.

We note that the choice of pseudo-inputs $\bar{\mathcal{X}}$ is not always intuitive or interpretable. In their original work, Snelson and Ghahramani [2006] proposed to choose these pseudo-inputs by maximizing the marginal likelihood. Other authors have proposed alternative methods of choosing pseudo-inputs based on minimizing the KL divergence [Titsias, 2009a,b, Damianou and Lawrence, 2013]. Such a fixed choice of pseudo-inputs results in a deterministic approximation to the covariance matrix [Titsias, 2009a, Lee et al., 2017].

2.3 Bayesian Additive Modeling and Back-fitting

Bayesian additive modeling [Hastie and Tibshirani, 1990, Chipman et al., 1998] is a flexible modeling technique that is widely adopted. In such an additive model, each model component captures only a portion of the overall response variability. The fitting of the additive Bayesian model through passing partial residuals to the next component follows the back-fitting scheme of Hastie and Tibshirani [2000]. Following Hastie and Tibshirani [2000], we can write an additive model with N components without intercept term in vector form as $\mathbf{y} = \sum_{j=1}^N \mathbf{f}_j + \epsilon$, $\epsilon \in N_n(\mathbf{0}_n, \sigma_\epsilon^2 \mathbf{I}_n)$, $\sigma_\epsilon^2 > 0$.

In each additive component, the mean function \mathbf{f}_j can be fitted based on the “ j -th residuals”, $\mathbf{r}_j = \mathbf{y} - \sum_{i \neq j} \mathbf{f}_i$. These residuals are used as data for the j -th component. Starting with a particular initial value, the back-fitting algorithm (Algorithm 3.1 in Hastie and Tibshirani [2000]) iterates until the joint distribution of all mean functions $(\mathbf{f}_1, \mathbf{f}_2, \dots, \mathbf{f}_N)$ stabilize. The particular model they fit to each additive component \mathbf{f}_j is the cubic spline model. Alternatively, we could fit each \mathbf{f}_j with a Gaussian process, where the update of \mathbf{f}_j conditioned on components $\{\mathbf{f}_i, i \neq j\}$ arises from $P(\mathbf{f}_j \mid \mathbf{y}, \mathbf{f}_1, \dots, \mathbf{f}_{j-1}, \mathbf{f}_{j+1}, \dots, \mathbf{f}_N) = P(\mathbf{f}_j \mid \mathbf{r}_j)$. This conditional likelihood allows us to implement the back-fitting algorithm and sample from the model. Further suggestions about the choice of priors for variance components and generalizations to generalized linear models are given in their research.

2.4 Localization Partition Scheme

Besides the idea of sparsification and Bayesian additive modeling, we will also incorporate the idea of localization via partitioning the input domain, which is another important technique in (approximating) GP regression. As pointed out by Chipman et al. [1998], such localized models recursively partition the input domain so that the probability distribution of the response is more homogeneous on a finer scale.

In this line of research, pioneering works were performed by Breiman [1984], Denison et al. [1998] and Chipman et al. [1998, 2010, 2016]. Other than tree-like partitioning schemes and its generalizations [Bentley, 1975, Pratola, 2016], there are alternative partition schemes for probabilistic modeling [Roy and Teh, 2008, Park and Huang, 2016, Gramacy and Apley, 2015]. Various choices of partition schemes on the input domain are discussed and studied in the local GP regression literature [Nguyen-Tuong et al., 2009, Park and Huang, 2016].

For the simplest case where the input domain is one dimensional, i.e. $[0, 1]$, a binary tree can be represented as 2^{r-1} equally divided intervals in the r -th layer of the tree [Bentley, 1975]. Various models using such partition schemes are proposed in the vast literature of Bayesian additive modeling. In Chipman et al. [1998], the data lying in each block defined by a partition scheme using a single binary tree is fitted to a component function of the model, i.e. on \mathbf{f}_j . This

associates the fitted mean function (or target) f_j with the data lying in a specific block. Subsequent works [Gramacy and Apley, 2015, Chipman et al., 2016, Pratola et al., 2018] in this direction brings fruitful results and demonstrates that assembling many simpler models over such block partitions can actually out-perform a single complex model fitted to the entire modeling domain.

As pointed out in Gramacy and Apley [2015] and Park and Apley [2018], such localization of the input-domain will fit and predict non-stationary datasets better. Furthermore, multi-scale features of a dataset can usually be well captured by introducing a hierarchical structure on the input domain [Fox and Dunson, 2012, Lee et al., 2017] or direct multi-scale approximations using appropriately chosen basis functions [Katzfuss, 2017, Katzfuss and Gong, 2017]. In our approach, capturing global and local features (or long-range and short-range dependencies) is accomplished through an RP structure, alleviating the issue of handling edge effects at partition boundaries. In the next section we introduce our model, where a trade-off between many simpler models and a single complicated model will naturally arise and becomes one of our research focuses.

3 Sparse Additive Gaussian Process Regression (SAGP)

3.1 The Recursive Partitioning Scheme

We consider a subdivision of the domain X based on a tree-like structure, and use the terminology for trees to describe one specific example. Figure 1 provides an example in the one-dimensional case, where $X = [0, 1]$. Each node corresponds to a subset A_j of X . Only the node at the first level, i.e., the root of the tree, corresponds to the whole domain ($A_1 = X$). As children of each node partition A_j into equal parts, nodes at lower levels correspond to smaller subsets. The collection of A_j corresponding to nodes at the same depth of the tree is referred to as a *layer*. In the example provided in Figure 1, we have three layers: $\mathcal{L}_1 = \{A_1\}$, $\mathcal{L}_2 = \{A_2, A_3\}$ and $\mathcal{L}_3 = \{A_4, A_5, A_6, A_7\}$. More formally, we define a *Recursive Partitioning* (RP) scheme as a collections of components $\{A_1, \dots, A_N\}$ and layers $\mathcal{L}_1, \dots, \mathcal{L}_L$ of these components satisfying the following properties:

1. (Nested) For a component $A_i \subset \mathbb{R}^d$ in the j -th layer \mathcal{L}_j , there exists a unique component $A_k \in \mathcal{L}_{j-1} \subset \mathbb{R}^d$ in the $(j-1)$ -layer \mathcal{L}_{j-1} such that $A_i \subset A_k$.
2. (Disjointedness, or non-overlapping) For two components A_i, A_k in the j -th layer \mathcal{L}_j such that $A_i \neq A_k$, their interiors do not intersect.
3. (Partitioning) For any layer $j = 1, \dots, L$, the union of the components belonging to the same layer satisfies $\cup_{i \in \mathcal{L}_j} A_i = X$.

In our case, we parameterize each component by its d -dimensional centroid μ_j and half-width $\sigma_{j,l}^2$ (where $\sigma_{j,l}^2 = \sigma_j^2$ is identical in each dimension for simplicity) as

$$A_j = B_{\mu_j}(\sigma_j) := \{x \in \mathbb{R}^d \mid |x^l - \mu_j^l| \leq \sigma_j, l = 1, \dots, d\}.$$

Each component is required to have a minimum of at least $m_j = m$ observations, so that it is possible to define a sparse GP with m_j pseudo-inputs in each $B_{\mu_j}(\sigma_j)$. Moreover, we require the collections $\bar{\mathcal{X}}^{(j)}$ of pseudo-inputs to be disjoint, so that each data point is only used once. Notably, RP schemes with several layers are unlikely to meet these conditions when a dataset is of limited size. Therefore, our approach is to first construct a complete RP scheme of desired depth, and then prune it back until the requirements for pseudo-inputs is satisfied. This deterministic RP scheme is what will be used by the SAGP model.

An example of constructing such an RP scheme is shown in Figure 1. Here we use $L = 3$ layers and $m_j = m = 3$ pseudo-inputs for each component. To demonstrate the pruning, we assume that the dataset has $n = 15$ observations, shown as the black dots in Figure 1(a). Note that there will be components $B_{\mu_j}(\sigma_j)$ containing less than m pseudo-inputs. For instance, in Figure 1(b), $B_{\mu_7}(\sigma_7) = [\frac{3}{4}, 1]$ only contains 2 observations. Second, it might be impossible to allocate distinct pseudo-inputs to some components and their ancestors. Although $B_{\mu_4}(\sigma_4)$ and $B_{\mu_5}(\sigma_5)$ both contain $m = 3$ points, it leaves their parent $B_{\mu_2}(\sigma_2)$ with no points to choose without repetition as shown in Figure 1(b). Therefore, we cannot fit an SGP model with $m = 3$ using all 7 active components.

While Figure 1(b) motivates why the full RP scheme with 3 layers needs to be pruned to be valid for this dataset, Algorithm 1 outlines the general algorithm for actually performing the pruning. Algorithm 1 essentially works by requiring that the total number of observations in component $B_{\mu_j}(\sigma_j)$ and all of $B_{\mu_j}(\sigma_j)$'s children satisfies the total required number of pseudo-inputs for these components. Starting from the bottom layer, Algorithm 1 recursively works up the tree, pruning sub-trees that do not satisfy this constraint on total number of observations. For instance, in Figure 1 the algorithm will work in following order:

The data points $\mathcal{X} = \mathcal{X}_n, (n = 15)$ are represented as dots on the intervals in the RP scheme \mathcal{B}_N . When we stipulate $m_j = m = 3$ in SAGP model, the colored points are selected as pseudo-input \mathcal{X}_j for different additive components. Different colors of points mean that the pseudo-inputs belong to different layers $\mathcal{L}_i, i = 1, 2, 3$.



Algorithm 1 “Pruning” algorithm for RP scheme.**Input** : RP partition scheme \mathcal{A} consisting of N components, Observed dataset $\{\mathcal{X}, \mathbf{y}\}$.**Output** : RP partition scheme \mathcal{A}' consisting of $N' \leq N$ components,

```

1 for  $l$  in  $L : 1$  do
2   for each component  $j$  in the  $l$ -th layer  $\mathcal{L}_l$  do
3     // We delete the children components from the bottom layer until there are
4     // sufficiently many observations for pseudo-input sampling.
5     for  $s$  in  $L : l$  do
6        $m_{req} \leftarrow$  Sum of the numbers of pseudo-inputs required for all active components contained in  $B_{\mu_j}(\sigma_j)$  in
7        $\mathcal{A}'$ .
8       if  $|\{x \in \mathcal{X} \mid B_{\mu_j}(\sigma_j)\}| \geq m_{req}$  then
9         break
10      else
11        Deactivate all the children components of component  $j$  from the model in  $s$ -th layer.
12      end
13    end
14  end
15 end

```

- Start from the layer 3 and examine $B_{\mu_7}(\sigma_7)$; deactivate this component since there are only 2 observations.
- Examine $B_{\mu_6}(\sigma_6), B_{\mu_5}(\sigma_5), B_{\mu_4}(\sigma_4)$; as they all contain at least $m = 3$ observations, keep them activated.
- Move to layer 2 and examine $B_{\mu_3}(\sigma_3)$, the number of observations required by the component and its children in RP scheme are
 3 (for active child $B_{\mu_6}(\sigma_6)$) + 3 (for $B_{\mu_3}(\sigma_3)$ itself) = $6 < 9$ observations. We keep it activated.
- Examine $B_{\mu_2}(\sigma_2)$; it contains
 $6 < 9 = 3$ (for active child $B_{\mu_4}(\sigma_4)$) + 3 (for active child $B_{\mu_5}(\sigma_5)$) + 3 (for $B_{\mu_2}(\sigma_2)$ itself) required observations. Therefore, we have to deactivate its children $B_{\mu_4}(\sigma_4), B_{\mu_5}(\sigma_5)$ from the bottom layer. Then we check again to ensure that $B_{\mu_2}(\sigma_2)$ contains 3 (for $B_{\mu_2}(\sigma_2)$ itself) observations. Since $B_{\mu_2}(\sigma_2)$ contains 6 observations and the condition is satisfied, we keep $B_{\mu_2}(\sigma_2)$ active.
- Move to layer 1 and examine $B_{\mu_1}(\sigma_1)$; it contains
 $15 > 12 = 3$ (for active child $B_{\mu_6}(\sigma_6)$) + 3 (for active child $B_{\mu_2}(\sigma_2)$) + 3 (for active child $B_{\mu_3}(\sigma_3)$) + 3 (for $B_{\mu_1}(\sigma_1)$ itself) observations, therefore there are sufficiently many observations for this component and its children $B_{\mu_3}(\sigma_3)$ and $B_{\mu_2}(\sigma_2)$ and we keep $B_{\mu_1}(\sigma_1)$ activated.
- Output the active components $B_{\mu_1}(\sigma_1), B_{\mu_2}(\sigma_2), B_{\mu_3}(\sigma_3)$ and $B_{\mu_6}(\sigma_6)$ as chosen in (c).

In Figure 1(c), we show the RP scheme after pruning, with one possible choice of exactly $m = 3$ pseudo-inputs in each component without repetition. The black points are not chosen as pseudo-inputs in this sampling of the pseudo-inputs, however any resampling for pseudo-inputs will meet the requirement that $m = 3$ pseudo-inputs per component under the proposed RP scheme.

3.2 SAGP Model

Given a (pruned) RP scheme, we propose an additive model for the response \mathbf{y} , where each component is an SGP model on the domain A_j . The *sparse additive Gaussian process* (SAGP) model with N additive components for observations $\{\mathcal{X}, \mathbf{y}\} = \{(x_i, y_i), i = 1, \dots, n\}$ can be written in the following additive vector form

$$\mathbf{y} = \sum_{j=1}^N \mathbf{f}_j + \boldsymbol{\epsilon}, \quad (3)$$

where $\mathbf{f}_j = (f_j(x_1), \dots, f_j(x_n))^T$ are the vector of values using the j -th model component and $\boldsymbol{\epsilon} \sim N_n(\mathbf{0}_n, \sigma_\epsilon^2 \mathbf{I}_n)$, $\sigma_\epsilon^2 > 0$. The function f_j is the function associated with the j -th component model A_j .

The model admits the same structure as general Bayesian additive regression models. To describe the SGP model of each component, let us denote the covariance kernel for the j -th component by $K^{(j)}$, $j = 1, \dots, N$. We use the

isotropic Gaussian covariance kernel supported inside A_j with parameters $\kappa^{(j)} = (\rho^{(j)}, \eta^{(j)})$:

$$K^{(j)}(\mathbf{x}, \mathbf{x}') := \frac{1}{\eta^{(j)}} \cdot \left(\rho^{(j)} \right)^{[(\mathbf{x} - \mathbf{x}')^T (\mathbf{x} - \mathbf{x}')]}, \forall \mathbf{x}, \mathbf{x}' \in A_j. \quad (4)$$

It is possible to assign different $\kappa^{(j)}$ for each component, but for simplicity we stipulate fixed positive $\rho^{(j)} = \rho_l$ for all components belonging to the same l -th layer in the prescribed RP scheme.

In the following discussion, for the j -th component corresponding to a specific partition block we use $\bar{\mathcal{X}}^{(j)}$ to denote the pseudo-inputs for the block,

$$\bar{\mathcal{X}}^{(j)} = \{\bar{\mathbf{x}}_1^{(j)}, \dots, \bar{\mathbf{x}}_{m_j}^{(j)}\} \subset B_{\mu_j}(\sigma_j). \quad (5)$$

Unlike a single sparse Gaussian process (SGP) which consists of a single component with pseudo-inputs, we consider multiple additive components and fit each additive component \mathbf{f}_j with the SGP model with the set $\bar{\mathcal{X}}^{(j)}$ consisting of m_j pseudo-inputs and corresponding pseudo-targets,

$$\bar{\mathbf{f}}_j = \left(f_j(\bar{\mathbf{x}}_1^{(j)}), f_j(\bar{\mathbf{x}}_2^{(j)}), \dots, f_j(\bar{\mathbf{x}}_{m_j}^{(j)}) \right)^T \in \mathbb{R}^{m_j}, j = 1, \dots, N. \quad (6)$$

Consider the pseudo-target vectors $\bar{\mathbf{f}}_1, \dots, \bar{\mathbf{f}}_N$ as parameters of our model, κ as the vector of parameters of the covariance kernels and σ_ϵ^2 as a parameter for the overall noise term. Let \mathcal{B}_N denote the pruned RP scheme with N components. Conditioned on the RP scheme and the corresponding pseudo-inputs $\bar{\mathcal{X}}^{(1)}, \dots, \bar{\mathcal{X}}^{(N)}$, the joint posterior of pseudo-targets and parameters in (3) can be written as:

$$\begin{aligned} & P(\bar{\mathbf{f}}_1, \dots, \bar{\mathbf{f}}_N, \kappa, \sigma_\epsilon^2 \mid \mathcal{B}_N, \mathbf{y}, \mathcal{X}, \bar{\mathcal{X}}^{(1)}, \dots, \bar{\mathcal{X}}^{(N)}) \propto \\ & P(\mathbf{y} \mid \bar{\mathbf{f}}_1, \dots, \bar{\mathbf{f}}_N, \kappa, \sigma_\epsilon^2, \mathcal{B}_N, \bar{\mathcal{X}}^{(1)}, \dots, \bar{\mathcal{X}}^{(N)}, \mathcal{X}) P(\bar{\mathbf{f}}_1, \dots, \bar{\mathbf{f}}_N \mid \mathcal{B}_N, \bar{\mathcal{X}}^{(1)}, \dots, \bar{\mathcal{X}}^{(N)}, \kappa) \times \\ & P(\kappa) P(\sigma_\epsilon^2) \end{aligned} \quad (7)$$

In effect, we view the choice of pseudo-inputs $\bar{\mathcal{X}}^{(1)}, \dots, \bar{\mathcal{X}}^{(N)}$ as nuisance parameters, and ultimately will integrate them out with respect to the prior $P(\bar{\mathcal{X}}^{(1)}, \dots, \bar{\mathcal{X}}^{(N)} \mid \mathcal{B}_N)$, taking the notation $d\bar{\mathbf{x}}^{m_j} = d\bar{\mathbf{x}}_1^{(j)} \times \dots \times d\bar{\mathbf{x}}_{m_j}^{(j)}$ to be integration over all pseudo-inputs in $\bar{\mathcal{X}}^{(j)}$, which gives posterior

$$\begin{aligned} P(\bar{\mathbf{f}}_1, \dots, \bar{\mathbf{f}}_N, \kappa, \sigma_\epsilon^2 \mid \mathcal{B}_N, \mathbf{y}, \mathcal{X}) &= \int p(\bar{\mathbf{f}}_1, \dots, \bar{\mathbf{f}}_N, \kappa, \sigma_\epsilon^2 \mid \mathcal{B}_N, \mathbf{y}, \mathcal{X}, \bar{\mathcal{X}}^{(1)}, \dots, \bar{\mathcal{X}}^{(N)}) \\ &\quad p(\bar{\mathcal{X}}^{(1)}, \dots, \bar{\mathcal{X}}^{(N)} \mid \mathcal{B}_N) d\bar{\mathbf{x}}^{m_1} \dots d\bar{\mathbf{x}}^{m_N} \end{aligned}$$

To fit and predict from our SAGP model, we derive closed form expressions for parameter posterior and predictive posterior distributions given observations. We also need to know the following distributions that are used in the Gibbs sampler for implementation:

1. Conditional likelihood of observations $P(\mathbf{y} \mid \bar{\mathbf{f}}_1, \dots, \bar{\mathbf{f}}_N, \kappa, \sigma_\epsilon^2, \mathcal{B}_N, \bar{\mathcal{X}}^{(1)}, \dots, \bar{\mathcal{X}}^{(N)}, \mathcal{X})$ given pseudo-targets.
2. Prior distribution for pseudo-targets. $P(\bar{\mathbf{f}}_1, \dots, \bar{\mathbf{f}}_N \mid \mathcal{B}_N, \bar{\mathcal{X}}^{(1)}, \dots, \bar{\mathcal{X}}^{(N)}, \kappa, \sigma_\epsilon^2)$.
3. Priors for $\kappa, \sigma_\epsilon^2, P(\kappa)P(\sigma_\epsilon^2)$.
4. Prior distribution for pseudo-inputs. $P(\bar{\mathcal{X}}^{(1)}, \dots, \bar{\mathcal{X}}^{(N)} \mid \mathcal{B}_N)$.

3.2.1 Conditional Likelihood of Observations

In this part, we derive the likelihood for response \mathbf{y} given all pseudo-targets $\bar{\mathbf{f}}_1, \dots, \bar{\mathbf{f}}_N$ from each additive component. We assume that the response \mathbf{y} has been standardized so that it has mean zero and variance one. With the notation introduced in (4), we can write down the covariance matrix between locations in $\mathcal{X}, \bar{\mathcal{X}}^{(j)}$ as below:

$$\mathbf{K}_n^{(j)} := \left[K^{(j)}(\mathbf{x}_k, \mathbf{x}_l) \right]_{k,l=1}^n, \quad (8)$$

$$\mathbf{K}_{m_j}^{(j)} := \left[K^{(j)}(\bar{\mathbf{x}}_k^{(j)}, \bar{\mathbf{x}}_l^{(j)}) \right]_{k,l=1}^{m_j}, \quad (9)$$

$$\mathbf{K}_{nm_j}^{(j)} := \left[K^{(j)}(\mathbf{x}_k, \bar{\mathbf{x}}_l^{(j)}) \right]_{k,l=1}^{n, m_j} = \left(\mathbf{K}_{m_j n}^{(j)} \right)^T. \quad (10)$$

We write for a general $\mathbf{x} \in \mathbb{R}^d$ that

$$\mathbf{k}^{(j)} := \left(K^{(j)}(\bar{\mathbf{x}}_1^{(j)}, \mathbf{x}), \dots, K^{(j)}(\bar{\mathbf{x}}_{m_j}^{(j)}, \mathbf{x}) \right)^T. \quad (11)$$

If we assume that the additive components are conditionally independent, for a single observation $y(\mathbf{x})$ we can derive (see Lemma 1 in Appendix B) its conditional likelihood

$P(y(\mathbf{x}) | \bar{\mathbf{f}}_1, \dots, \bar{\mathbf{f}}_N, \boldsymbol{\kappa}, \sigma_\epsilon^2, \mathcal{B}_N, \bar{\mathcal{X}}^{(1)}, \dots, \bar{\mathcal{X}}^{(N)}, \mathcal{X})$. In vector form, this becomes,

$$P(\mathbf{y} | \bar{\mathbf{f}}_1, \dots, \bar{\mathbf{f}}_N, \boldsymbol{\kappa}, \sigma_\epsilon^2, \mathcal{B}_N, \bar{\mathcal{X}}^{(1)}, \dots, \bar{\mathcal{X}}^{(N)}) = N_n \left(\mathbf{y} \left| \sum_{j=1}^N \mathbf{K}_{nm_j}^{(j)} \left(\mathbf{K}_{m_j}^{(j)} \right)^{-1} \bar{\mathbf{f}}_j, \sigma_\epsilon^2 \mathbf{I}_n + \sum_{j=1}^N \boldsymbol{\Lambda}_n^{(j)} \right. \right) \quad (12)$$

where the matrix $\boldsymbol{\Lambda}_n^{(j)} := \text{diag} \left(K_{ii}^{(j)} - \mathbf{k}_i^{(j)T} \left(\mathbf{K}_{m_j}^{(j)} \right)^{-1} \mathbf{k}_i^{(j)} \right)_{n \times n}$ takes the diagonal form, with $\mathbf{k}_i^{(j)}$ defined in (11) but with $\mathbf{x} = \mathbf{x}_i \in \mathcal{X}$.

3.2.2 Prior Distribution of Pseudo-targets

The conditional distribution of pseudo-targets given pseudo-inputs and hyper-parameters is straight-forward. Following Snelson and Ghahramani [2006], the pseudo-targets $\bar{\mathbf{f}}_1, \dots, \bar{\mathbf{f}}_N$ are assumed to be conditionally independent when conditioning on pseudo-inputs $\bar{\mathcal{X}}^{(1)}, \dots, \bar{\mathcal{X}}^{(N)}$ and distributed as Gaussian distributions with prescribed kernels,

$$\begin{aligned} P(\bar{\mathbf{f}}_1, \dots, \bar{\mathbf{f}}_N | \mathcal{B}_N, \bar{\mathcal{X}}^{(1)}, \dots, \bar{\mathcal{X}}^{(N)}, \mathcal{X}, \boldsymbol{\kappa}) &= \prod_{j=1}^N P(\bar{\mathbf{f}}_j | \mathcal{B}_N, \bar{\mathcal{X}}^{(j)}, \mathcal{X}, \boldsymbol{\kappa}^{(j)}) \\ &= \prod_{j=1}^N N_{m_j} \left(\bar{\mathbf{f}}_j \middle| \mathbf{0}_{m_j}, \mathbf{K}_{m_j}^{(j)} \right) \end{aligned} \quad (13)$$

where we recall the notation $\boldsymbol{\kappa}^{(j)}$ is the j -th component for the parameter $\boldsymbol{\kappa}$ that parameterizes the covariance function $K^{(j)}$ used in the j -th additive component in \mathcal{B}_N .

3.2.3 Prior Distributions of Pseudo-inputs

In our model, we choose a discrete uniform distribution from the available inputs in each component $B_{\mu_j}(\sigma_j)$ as the pseudo-input prior. Define the index set for the components

$$\mathcal{I}_j := \{k \neq j \text{ such that the support of } B_{\mu_k}(\sigma_k) \text{ is contained in } B_{\mu_j}(\sigma_j)\} \subset \{1, \dots, N\},$$

and we also define the collection of children components of $\bar{\mathcal{X}}^{(j)}$ as

$$\mathcal{C}(\bar{\mathcal{X}}^{(j)}) := \{B_{\mu_k}(\sigma_k) | k \in \mathcal{I}_j\}, j = 1, \dots, N.$$

For example, in Figure 1(c) the $\mathcal{C}(\bar{\mathcal{X}}^{(1)}) := \{B_{\mu_2}(\sigma_2), B_{\mu_3}(\sigma_3), B_{\mu_6}(\sigma_6)\}$, $\mathcal{C}(\bar{\mathcal{X}}^{(2)}) := \emptyset$, $\mathcal{C}(\bar{\mathcal{X}}^{(3)}) := \{B_{\mu_6}(\sigma_6)\}$. Then we know that the pseudo-inputs that are already used in the children components of the component corresponding to $B_{\mu_j}(\sigma_j)$ can be written as $\bar{\mathcal{X}}_{\text{children}}^{(j)} := \cup_{k \in \mathcal{I}_j} \bar{\mathcal{X}}^{(k)}$ and

$$P(\bar{\mathcal{X}}^{(1)}, \dots, \bar{\mathcal{X}}^{(N)} | \mathcal{B}_N) = \prod_{\ell=1}^L \prod_{B_{\mu_j}(\sigma_j) \in \mathcal{L}_\ell} P(\bar{\mathcal{X}}^{(j)} | \mathcal{C}(\bar{\mathcal{X}}^{(j)})) \quad (14)$$

$$P(\bar{\mathcal{X}}^{(j)} | \mathcal{C}(\bar{\mathcal{X}}^{(j)})) = \prod_{i=1}^{m_j} P(\bar{\mathbf{x}}_i^{(j)} | \mathcal{C}(\bar{\mathcal{X}}^{(j)})) \quad (15)$$

$$P(\bar{\mathbf{x}}_i^{(j)} | \mathcal{C}(\bar{\mathcal{X}}^{(j)})) = \text{Discrete Uniform} \left(\left\{ \mathbf{x} \in \mathcal{X} \setminus \bar{\mathcal{X}}_{\text{children}}^{(j)} \right\} \right), j = 1, \dots, N \quad (16)$$

In the expression above, we essentially draw a random sample from all those observed locations that have not been selected as pseudo-inputs of any components in lower layers. This choice of prior is subject to the (pruned) RP scheme. The alternative, for example continuous uniform prior over each component domain, or sampling accordingly to design theoretic considerations [Pratola et al., 2019] are possible. In Snelson and Ghahramani [2006, 2007], a random choice

of pseudo-inputs is also suggested when maximization of the marginal likelihood is not realistic. With the partitioning scheme, we extend the random choice of pseudo-inputs subject to the RP partition scheme.

Unlike other sparse GP approaches, with this random sampling scheme within local input domains, $B_{\mu_j}(\sigma_j)$, we capture the uncertainty of pseudo-input selection and propagate this uncertainty to the posterior. Note that with this choice of prior, there will not be two identical pseudo-inputs selected with probability one. The sampling of the pseudo-inputs is summarized in Algorithm 2.

3.2.4 Prior Distributions of Hyper-parameters

We place an inverse gamma prior on the noise variance, σ_ϵ^2 , in order to make use of the Gaussian-inverse gamma conjugacy,

$$\sigma_\epsilon^2 \sim \text{InverseGamma}(\alpha_\epsilon, \beta_\epsilon). \quad (17)$$

We assume independent inverse gamma priors on each scale parameter $\eta^{(j)}$. For the j -th component that lie in the l -th layer of the RP scheme,

$$P(\boldsymbol{\kappa}) = P(\boldsymbol{\kappa}^{(1)}, \dots, \boldsymbol{\kappa}^{(j)}) = \prod_{\ell=1}^L \prod_{B_{\mu_j}(\sigma_j) \in \mathcal{L}_\ell} P(\eta^{(j)} \mid \alpha_\eta^l, \beta_\eta^l), \quad (18)$$

$$\text{where } \eta^{(j)} \sim \text{InverseGamma}(\alpha_\eta^l, \beta_\eta^l) \quad (19)$$

and the hyper-parameters $\alpha_\eta^l, \beta_\eta^l > 0, l = 1, \dots, L$ are assumed to be the same for the components within the same layer but different for different layers of the RP scheme.

Priors on σ_ϵ^2 and $\bar{\mathbf{f}}$ are meant to utilize the normal conjugacy. But the prior on η_j will not have conjugacy but simply a canonical choice. The hyper-parameters in these priors can be calibrated according to the data. For example we can calibrate the scale of kernels by adjusting $\alpha_\eta^l, \beta_\eta^l$ to the scale of observations. In practice we suggest choosing the means of priors for the components of each layer $\frac{\beta_\eta^l}{\alpha_\eta^l - 1}, l = 1, \dots, L$ to be of different magnitudes. For example, $\frac{\beta_\eta^l}{\alpha_\eta^l - 1} = 10^{-1}, 10^{-10}, 10^{-50}$ for $l = 1, 2, 3$ in a RP scheme with $L = 3$ layers. We could also think to have different parameters $\eta^{(j)}$ in the covariance kernels for different components, which allows the model to capture smooth and wiggly behaviors (or short-range and long-range dependency) of the response.

The apriori choice of the hyper-parameters $\rho^{(j)}$ is probably the most tricky part of our model. On one hand, the maximum likelihood estimates based on the data and full likelihood (7) can serve as a reference of choosing suitable hyper-parameters $\rho^{(j)}$ but its calculation is usually not numerically stable and its analytic form is intractable. On the other hand, the (scaled) Pearson correlation coefficients seem to be a good reference when making choice of ρ in the Gaussian kernel (4). But empirically, we determine that we choose the same ρ_l for all components in the same layer and enforce a decay such that $\rho_l \gg \rho_{l+1}$. In particular, we set $\rho_1 = 10^{-1}, \rho_L = 10^{-50}$ and the intermediate values $\rho_l, l = 1, \dots, L-1$ to be equally spaced between ρ_1 and ρ_L on the logarithm (base 10) scale. The choice reflects the observation that the variability decreases along the layer since we assume that the components in the top layer capture the global pattern and the variability should be larger; the components in the bottom layer captures the local details and the variability should be smaller. This implies an apriori assumption of decaying multi-scale additive features of the true response, so that correlations at a component with a smaller (more localized) domain also tend to be smaller. The requirement $\rho_l \gg \rho_{l+1}$ helps us to distinguish the strength of correlation between different layers of the RP scheme. Alternatively, these $\rho^{(j)}$ can be modeled as real parameters, at an increased computation cost and slower mixing of the MCMC.

3.2.5 Full Conditional Distribution of Pseudo-targets

We apply Bayes theorem on the $\bar{\mathbf{f}}_j$ in order to yield its full conditional distribution from (12) and (13) and the conditional independence assumption,

$$\begin{aligned} P(\bar{\mathbf{f}}_j | \mathbf{y}, \mathcal{X}, \bar{\mathbf{f}}_1, \dots, \bar{\mathbf{f}}_{j-1}, \bar{\mathbf{f}}_{j+1}, \dots, \bar{\mathbf{f}}_N, \mathcal{B}_N, \bar{\mathcal{X}}^{(1)}, \dots, \bar{\mathcal{X}}^{(N)}, \boldsymbol{\kappa}, \sigma_\epsilon^2) \\ \propto P(\mathbf{y} | \bar{\mathbf{f}}_1, \dots, \bar{\mathbf{f}}_N, \mathcal{B}_N, \bar{\mathcal{X}}^{(1)}, \dots, \bar{\mathcal{X}}^{(N)}, \boldsymbol{\kappa}, \sigma_\epsilon^2) \times \\ P(\bar{\mathbf{f}}_j | \mathcal{X}, \mathcal{B}_N, \bar{\mathcal{X}}^{(j)}, \boldsymbol{\kappa}, \sigma_\epsilon^2) \end{aligned} \quad (20)$$

$$\begin{aligned} = N_n \left(\mathbf{r}_j | \mathbf{K}_{nm_j}^{(j)} \left(\mathbf{K}_{m_j}^{(j)} \right)^{-1} \bar{\mathbf{f}}_j, \boldsymbol{\Lambda}_n^{(j)} + \sigma_\epsilon^2 \mathbf{I}_n \right) \times \\ N_{m_j} \left(\bar{\mathbf{f}}_j | \mathbf{0}_{m_j}, \mathbf{K}_{m_j}^{(j)} \right), \text{ where } \mathbf{r}_j = \mathbf{y} - \sum_{l \neq j} \mathbf{K}_{nm_l}^{(l)} \left(\mathbf{K}_{m_l}^{(l)} \right)^{-1} \bar{\mathbf{f}}_l \end{aligned} \quad (21)$$

Using the normal-normal conjugacy, we can identify the mean and variance of this normal distribution $\bar{\mathbf{f}}_j$ | $\text{Mean}_j, \text{Var}_j$, as below (detailed derivations are provided in Appendix B) :

$$\begin{aligned} \text{Mean}_j &= \mathbf{K}_{m_j}^{(j)} \mathbf{Q}_{m_j}^{(j)-1} \mathbf{K}_{m_j n}^{(j)} \left(\boldsymbol{\Lambda}_n^{(j)} + \sigma_\epsilon^2 \mathbf{I}_n \right)^{-1} \mathbf{r}_j, \\ \text{Var}_j &= \mathbf{K}_{m_j}^{(j)} \mathbf{Q}_{m_j}^{(j)-1} \mathbf{K}_{m_j}^{(j)}, \\ \text{where } \mathbf{Q}_{m_j}^{(j)} &= \mathbf{K}_{m_j}^{(j)} + \mathbf{K}_{m_j n}^{(j)} \left(\boldsymbol{\Lambda}_n^{(j)} + \sigma_\epsilon^2 \mathbf{I}_n \right)^{-1} \mathbf{K}_{nm_j}^{(j)}. \end{aligned} \quad (22)$$

Although we still need to invert an $n \times n$ matrix $\boldsymbol{\Lambda}_n^{(j)} + \sigma_\epsilon^2 \mathbf{I}_n$, it is a diagonal matrix and hence its computational cost will be $\mathcal{O}(n)$.

3.2.6 Full Conditional Distribution of Noise Variance

As we mentioned in the previous section, we want to make use of the Gaussian-inverse gamma conjugacy. For the observation of sample size n , by conjugacy, the distribution σ_ϵ^2 is again inverse gamma

$$P(\sigma_\epsilon^2 | \mathbf{y}, \mathcal{X}, \bar{\mathbf{f}}_1, \dots, \bar{\mathbf{f}}_N, \mathcal{B}_N, \bar{\mathcal{X}}^{(1)}, \dots, \bar{\mathcal{X}}^{(N)}, \boldsymbol{\kappa}) \sim \text{InverseGamma}(\alpha_\epsilon + \frac{n}{2}, \beta_\epsilon + \frac{1}{2}(\mathbf{y} - \hat{\mathbf{y}})^T(\mathbf{y} - \hat{\mathbf{y}})), \quad (23)$$

where $\hat{\mathbf{y}} := \sum_{j=1}^N \mathbf{K}_{nm_j}^{(j)} \left(\mathbf{K}_{m_j}^{(j)} \right)^{-1} \bar{\mathbf{f}}_j$ is the ‘‘fitted value’’ from the SAGP model. We can directly sample this parameter using a Gibbs step.

3.2.7 Sampling Algorithm

SAGP is fitted by a Metropolis-Hastings Markov chain Monte Carlo (MCMC) algorithm [Alan E. Gelfand, 1990, Robert and Casella, 2011]. For each additive component of the model, we have to use the partial residuals \mathbf{r}_j defined in (21). This step is from the back-fitting scheme designed for fitting additive Bayesian models [Hastie and Tibshirani, 2000].

From the likelihood derivations presented in section 3.2.5, we know that $\bar{\mathbf{f}}_j$ can be directly sampled from their conditional distributions for each $j = 1, \dots, N$ components. The difficulty in this step is to compute the $\text{Mean}_j, \text{Var}_j$ in (22). As mentioned earlier, the main computational cost occurs in the inversion of the covariance matrices in section 3.2.1, which have been reduced compared to a full GP covariance matrix. Numerical instability in inversion of these matrices may cause additional problems, so we adopted the Cholesky decomposition method with diagonal perturbation to solve this instability problem as in Rasmussen and Williams [2006]. For each η_j we do not have normal conjugacy, therefore an adaptive Metropolis-Hasting step is used for sampling η_j [Banerjee et al., 2012].

The advantage of using such a fully Bayesian model is that the uncertainty quantification comes naturally with the posterior samples from the sampler. Our posterior inference below can be based on all these posterior samples. The algorithm for overall sampling is presented in Algorithm 3.

3.2.8 Tuning Parameters and Complexity

The trade-off between number of layers L in the RP scheme and the number of pseudo-inputs m_j is also central to the SAGP model. In previous SGP modeling [Snelson and Ghahramani, 2006, 2007, Lee et al., 2017], it is observed that to get a better fit of the SGP model we need to increase the number of pseudo-inputs m . On the other hand, for

Algorithm 2 Sampling algorithm for pseudo-inputs subject to RP scheme.

Input : RP partition scheme consisting of N components, Observed dataset $\{\bar{\mathcal{X}}, \mathbf{y}\}$.

Output : Sample of $\bar{\mathcal{X}}^{(j)}, j = 1, \dots, N$ subject to the RP scheme.

```

1 Initialize all  $\bar{x} \in \mathcal{X}$  as eligible locations.
2 for  $j$  in  $N : 1$  do
3   Eligible  $\mathcal{X}$ : the observations  $\mathcal{X}$  that lie in the  $j$ -th component.
4   Available  $\mathcal{X}$ : the observations  $\mathcal{X}$  that are not deactivated in all previous components  $1, \dots, (j - 1)$ .
5   Sample a random sample  $\bar{\mathcal{X}}^{(j)} \subset \mathcal{X} \subset \mathbb{R}^d$  of size  $m_j$  from  $\{\text{Eligible } \mathcal{X}\} \cap \{\text{Available } \mathcal{X}\}$ .
6   Deactivate those  $\bar{x}$  that has been sampled from the previous step.
7 end
```

tree-like partition based modeling [Chipman et al., 1998, 2016, Pratola et al., 2018], it is observed that the more additive components the model has, the better fit we can expect. In our SAGP model, both factors (number of pseudo-inputs $m_j = m$ in each component; number of layers, L , in RP scheme) show an interesting trade-off. Increasing the number of layers may counter-act the effect of decreasing the number of pseudo-inputs; Increasing the number of pseudo-inputs may counter-act the effect of decreasing the number of layers in RP scheme. In practice, we tune the choice of number of layers using cross-validation.

Consider the complexity of inverting the covariance matrix in an SAGP model and other types of GP models. We already mentioned above that for a full GP model based on \mathcal{X}_n the complexity is of order $\mathcal{O}(n^3)$; for SGP model with m pseudo-inputs based on \mathcal{X}_n the complexity is of order $\mathcal{O}(nm^2)$ [Snelson and Ghahramani, 2006]. For each additive component in our SAGP model, since it is essentially an SGP model we know that the complexity of inverting its matrix is $\mathcal{O}(nm_j^2) = \mathcal{O}(nm^2)$. There will be N additive components in our SAGP model. And the overall complexity is given in the following proposition.

Proposition 1 *For an RP scheme on input-domain $[0, 1]^d$, with b_i -ary tree [Storer, 2012] in the i -th dimension, the complexity of fitting an L -layer SAGP model with m pseudo-inputs for each component to a sample of size n is $\mathcal{O}\left(\sum_{\ell=1}^L \prod_{i=1}^d b_i^{\ell-1} \cdot n \cdot m^2\right)$.*

Proof See Appendix C. ■

Therefore if we stipulate our complexity at a certain order $\mathcal{O}(n^3)$ for a fixed dataset \mathcal{X}_n , then it is clear that we must ensure that $\mathcal{O}\left(\sum_{\ell=1}^L \prod_{i=1}^d b_i^{\ell-1} m^2\right) \asymp \mathcal{O}(n^2)$. Then the trade-off becomes explicit because when L increases m must decrease and vice versa. For $N \sim \mathcal{O}(1)$ this complexity reduces to SGP complexity. This complexity requires a fixed number of additive components. We will revisit this *component number pseudo-input trade-off* in our example analyses.

4 Simulation Study

4.1 Design

To evaluate the performance of our methodology and compare it to competing approaches, we run a family of simulations. We focus on the one-dimensional case ($d = 1$) and we simulate from a GP with mean function

$$f(x) = -5 - 6x^3 + 30(x - .5)^2 + 3 \exp(2x - 1) + 3x^2 \sin(12\pi x) + \cos(6\pi x),$$

which is represented in Figure 2 in the interval $[0, 1]$. We generate a sample of $n = 200$ locations from a uniform distribution on $[0, 1]$ and we define the observed responses as $y_i = f(x_i) + \epsilon_i$ for all $x_i \in \mathcal{X}$, with ϵ_i sampled as independent noise with distribution $N_1(0, 0.1)$. The data are split into training and testing sets, with sizes 150 and 50, respectively. We consider two scenarios. In the first scenario, the testing set is selected at random. In the second scenario, the testing set is chosen as the subset with locations in the central portion of the $[0, 1]$ interval, by selecting the 50 data points with x_i closest to 0.5. Figure 2 shows one example of data generated with such a procedure.

We generate 1000 batches of datasets. In each dataset, we apply three configurations of the SAGP model, using different choices of number of pseudo-inputs m and layers L : (i) $m = 5, L = 4$; (ii) $m = 10, L = 3$; (iii) $m = 15, L = 3$. In particular, the number of layers is selected as the largest possible value given the choice of m and the sample size n . We compare the SAGP models to the following methods:

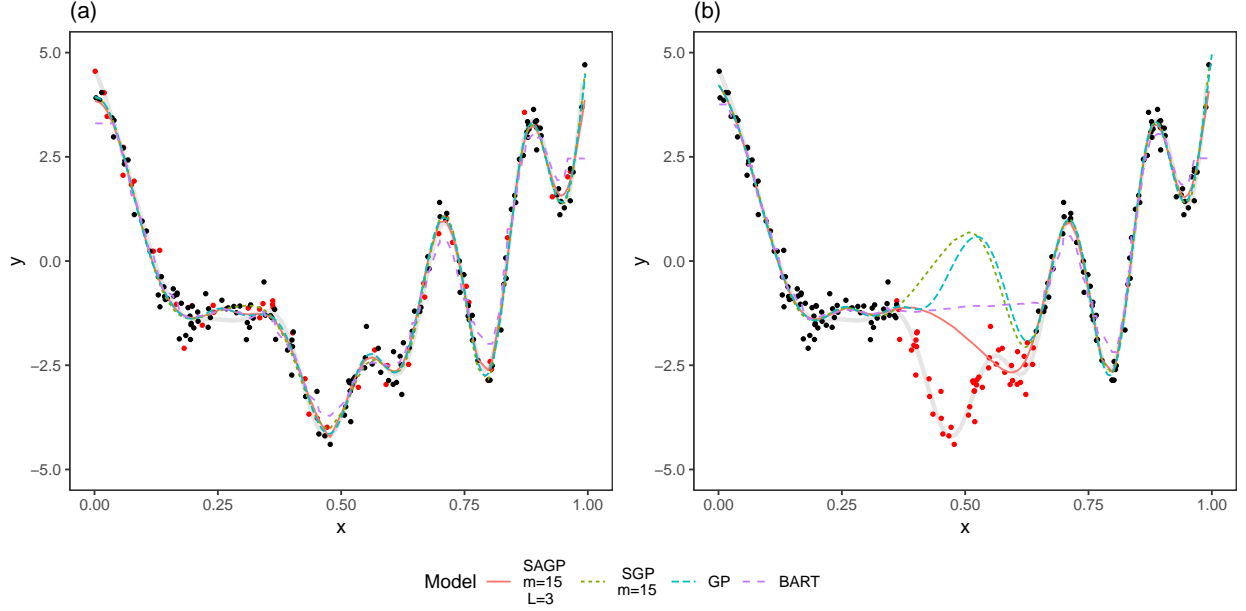


Figure 2: Example of data generated in the simulation study. The gray, bold, curve represents the true mean function $f(x)$. Training and testing sets are represented as black and red points. Panels (a) and (b) show the scenarios where the testing set is chosen at random or in the central portion of the $[0, 1]$ interval, respectively. The posterior predictive functions of four models, fit on the training portion of the data, are provided in both panels.

- Full GP regression. We use the implementation of GP regression model in the R package *DiceKriging* by Roustant et al. [2012].
- SGP regression. We consider the choices $m = 5$, $m = 10$ and $m = 15$ and use the implementation of SGP in the Matlab library *SPGP* accompanying the paper by Snelson and Ghahramani [2006].
- Bayesian Additive Regression Trees (BART) Chipman et al. [1998, 2010], Pratola et al. [2018]. We used the default number of trees as specified in Chipman et al. [2010] and the implementation at <http://bitbucket.org/mpratola/openbt>.

For each batch of generated dataset and type of testing set, the methods are fit on the training portion of the data and applied to each location x_i of the testing set, computing the predicted value $\hat{y}(x_i)$ (whose definition is in Section 3.2.6) of the mean function and the 95% prediction interval (PI) for y_i . The performance of the estimators of the mean function is evaluated in terms of mean squared error (MSE), i.e., the average of $(y_i - \hat{y}(x_i))^2$ over the test set. To assess the appropriateness of the uncertainty quantification, we compute the coverage of the PIs and compare it to the nominal prediction level. Finally, we compare the methods in terms of average value of interval score, which is a summary measure to assess the quality of prediction intervals [Gneiting and Raftery, 2007]. Given a $(1 - \alpha)100\%$ PI for y_i with extremes (l_i, u_i) , the interval score at y_i is defined as

$$s_\alpha(l_i, u_i; y_i) = (u_i - l_i) + \frac{2}{\alpha}(l_i - y_i)\mathbf{1}(y_i < l_i) + \frac{2}{\alpha}(y_i - u_i)\mathbf{1}(y_i > u_i).$$

We choose this metric to jointly evaluate a family of intervals in terms of precision (i.e. the width of the intervals) and accuracy (i.e., the coverage of the true value). Notably, low score values are a sign of good performance.

4.2 Results

Figure 3 summarizes the resulting MSEs, PI coverages and averages of the interval scores across the 1000 batches generated datasets.

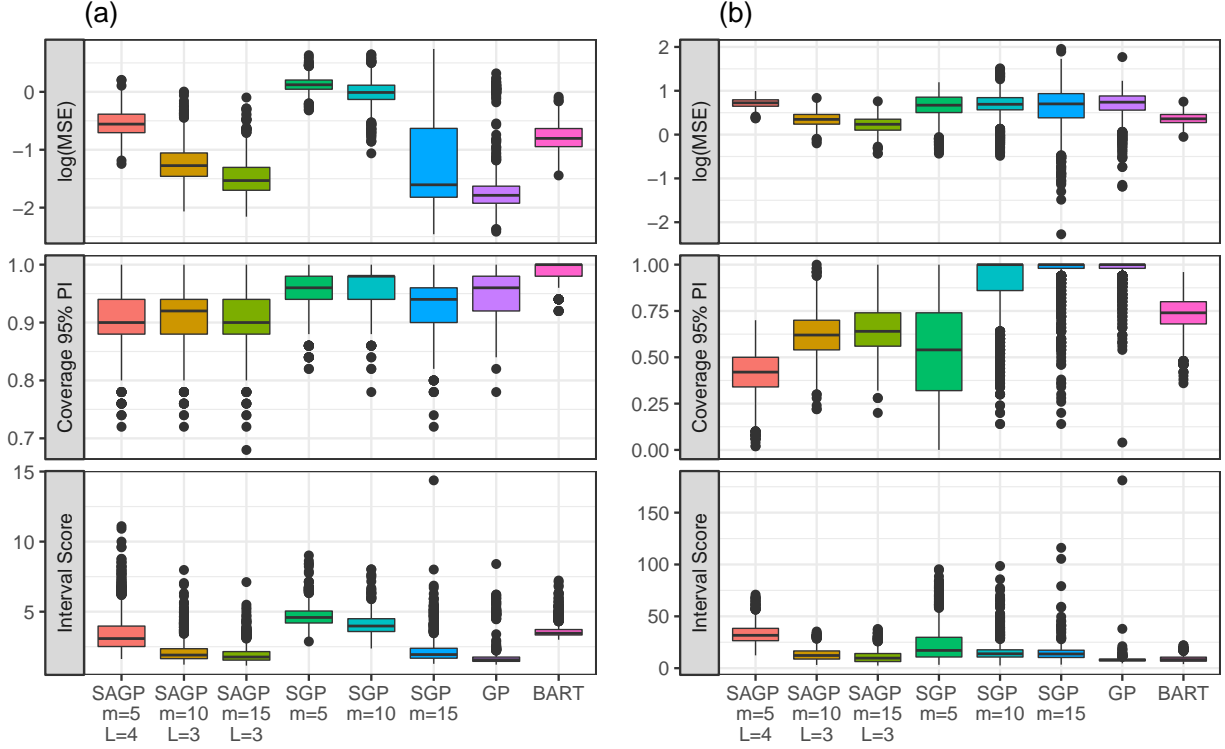


Figure 3: MSE on the \log_{10} scale (top panels), coverage (central panels) and interval score (bottom panels) over the 1000 simulated datasets. Panels (a) and (b) show the results in the case where the testing set is chosen at random over $[0, 1]$ or in the central portion of the $[0, 1]$ interval, respectively.

4.2.1 Random Testing Set

The panel (a) of Figure 3 provides the results in the scenario with testing set selected at random. In terms of MSE, both the SAGP and SGP models perform better with larger values of m . In particular, the full GP model attains the smallest MSEs. The SAGP models with $m = 5$ and 10 perform better than the SGP models with the same number of pseudo-inputs. For $m = 15$, the median MSEs in the SAGP and SGP models are similar, but the performance of the SAGP model is more consistent across simulations (the upper quartile of SAGP with $m = 15$ is considerably smaller than the one of SGP with $m = 15$). With the considered configuration of the parameters, the BART model performs slightly better than the SAGP model with $m = 5$, but worse than the SAGP model with $m = 10$ and $m = 15$.

The coverage of the 95% PIs is close to the nominal level for all the methods except for BART. The PIs of the SAGP model appear to be slightly too narrow, as most of the coverages are a little lower than .95. SGP and GP models show coverages perfectly matching the nominal value. However, the BART model produces overly wide PIs, as the median coverage is 100%.

The ranking of the methods in terms of interval score is similar to the one based on the MSE. Again, better performances are attained by SAGP and SGP models with larger values of m . The SAGP models with $m = 10$ and $m = 15$ perform better than all the other methods, except for the full GP model.

4.2.2 Interval Testing Set

The panel (b) of Figure 3 provides the results of the simulations in the scenario where the testing set is located in the central portion of the $[0, 1]$ interval. Notably, this prediction problem is much harder than the one evaluated by the previous scenario, as the models are forced to a certain degree of extrapolation due to the lack of data. This is clear from the much larger values of MSE attained by all the methods in this scenario. Interestingly, while the SAGP model results in smaller MSE values for larger m , the same behavior is not observed for SGP models. In particular, SGP and GP models show similar performances, which are worse than SAGP with $m = 10$ and 15 and BART. The

additive decomposition in global and local components is an advantage of the SAGP model in this scenario. The global components, corresponding to the first layers of the model, are expected to capture the overall trend of the underlying function, even in the central portion of the domain where there is no data.

All the methods perform poorly in terms of coverage of the PIs. The coverages of SAGP, BART and SGP models with $m = 5$ are considerably lower than the nominal level. On the other side of the spectrum, GP and SGP models with $m = 10$ and 15 show coverage of 100% most of the times, implying that the corresponding PIs are overly wide. All three methods also show very low coverages in several instances.

With respect to the interval score, the methods that appear to perform best are SAGP with $m = 15$, GP and BART. These methods attain the smallest scores for different reasons. On the one hand, SAGP and BART models show better predictive performances (smaller MSE) but PIs too narrow (coverage lower than nominal level). On the other hand, the GP model performs worse in terms of point estimation (larger MSE) but the associated PIs are so wide that they cover the observed values almost all of the times (coverage higher than nominal level).

5 Real-world Data Applications

We applied the SAGP model to two different real-world datasets with dimension $d = 1$ and $d = 2$, respectively. The difference between real datasets and simulation dataset is that we do not know the underlying truth. Explaining real-world data can also demonstrate the interpretability of our model.

5.1 Heart Rate Data

GP regression is well-suited to model streams of vital signs, such as heart rate (HR) recordings, because one can account for random noise and “knowledge of the generative physiology” [Colopy et al., 2016]. Current research focuses on identifying patterns of HR streams of critical patients, to detect signals of deterioration [Almeida and Nabney, 2016]. In other contexts, the HR can be used to evaluate the level of physical preparation and design training/rehabilitation activities [Zakynthinaki, 2015]. Notably, HR streams often consist of a massive amount of data points. This is because clinical researchers are interested in detecting patterns over long time intervals, and the measurements are taken with high frequency. Moreover, recording the HR in beats/minute is very easy and can be performed with cheap wearable devices. In this context, the large amount of available data makes standard GP regression computationally expensive.

We apply the proposed SAGP regression to model HR data. We use data recorded for a clinical study investigating the HR kinetic [Zakynthinaki, 2015]. A single 33-year old runner was asked to run on a treadmill at constant speed. The HR (in beats/minute) was recorded for about 7 minutes from the beginning of the exercise. After the exercise, the HR of the subject was measured for about 10 minutes during the recovery. The experiment was repeated four times, varying the speed of the exercise ($v = 13.4, 14.4, 15.7$ and 17 km/h). For our illustrative purposes, we use the data of the exercise performed at speed $v = 13.4$ km/h, which are graphically represented in Figure 5. When the exercise starts (at time 0), the HR increases to a frequency of around 140 beats/minutes. The physical exercise ends after 450 seconds and, during the recovery phase, the HR returns to the basal frequency. The stream consists of 1,664 recordings.

We consider SAGP models with $m = 5$ and $m = 10$ pseudo-inputs. For each value, we use 10-fold cross-validation to select the number of layers L . We apply this procedure for values of L from 1 to 6 and compute the MSE of the out-of-sample predictions. Figure 4(a) shows the computed MSEs (on \log_{10} scale). We select the value of L where the predictive performance levels off, i.e., the values $L = 4$ and 3 for $m = 5$ and 10 , respectively. There is an intuitive trade-off between the values of pseudo inputs m and the number of layers L . If the goal is to maximize the predictive performance, smaller values of m require SAGP setups with more layers and, consequently, more additive components.

Figure 5 provides the result of the fit of the SAGP model with $m = 10$ and $L = 3$. All of the 7 additive components of the three-layer partition scheme are active, due to the sufficient availability of data. Panel (a) shows the posterior means of each component and the corresponding 95% quantile-based credible intervals on 100 equispaced locations on the support of the data. Interestingly, the sole component on the first layer (component 1) captures the overall trend of the frequencies during the physical activity and the steep decrease in HR values after the interruption of the exercise. The remaining components capture other features of the data on a finer scale. Panel (b) of the figure provides the posterior predictive mean function, evaluated on the same 100 locations, and the corresponding 95% prediction intervals. Notably, the SAGP model successfully captures the apparent non-stationary behavior of the data and appears to provide an accurate estimate of the observed noise. The same output for the model with $m = 5$ and $L = 4$ is provided in Appendix D.

Figure 4: (a) Out-of-sample MSE (on \log_{10} scale) attained by different models fitted on 1 dimensional heart-rate dataset with $m = 5, 10$ and $L = 1, \dots, 6$.
 (b) Out-of-sample MSE (on \log_{10} scale) attained by different models fitted on 2 dimensional temperature dataset with $m = 5, 10, 15, 20, 25$ and $L = 1, \dots, 4$. For any $L > 4$, our pruning algorithm will reduce it to $L = 4$; for $m = 25$ our pruning algorithm will reduce SAGP model to $L = 3$

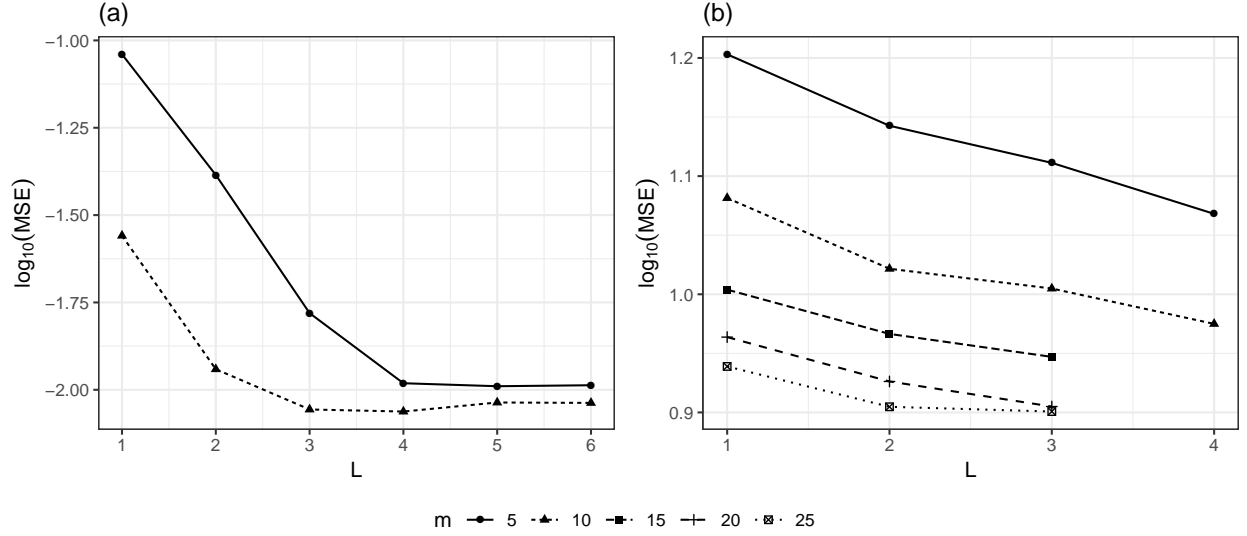
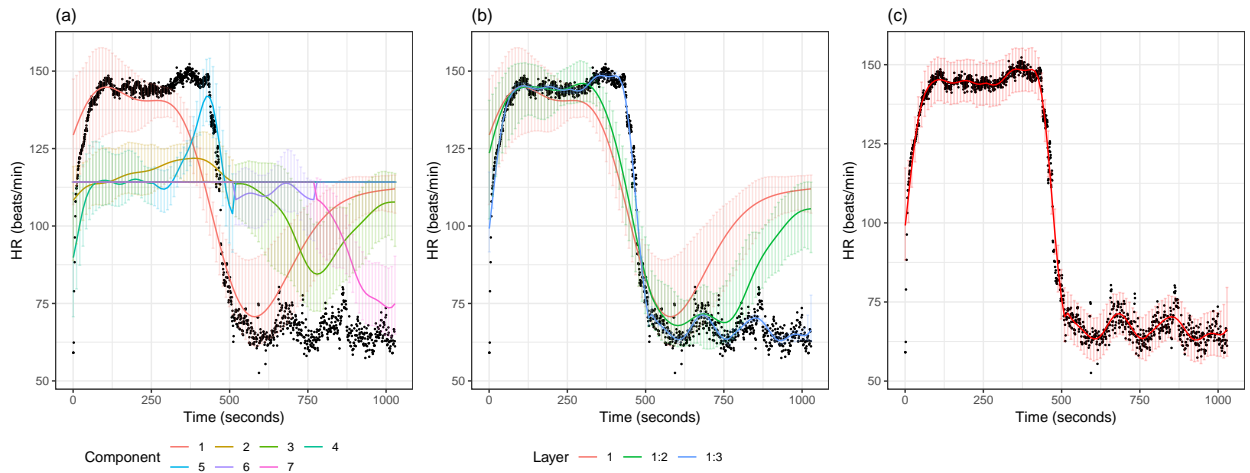


Figure 5: The panels show the observed HR values over time as black dots and results about the fit of the SAGP model with $m = 10$ and $L = 3$. Panel (a) shows the posterior means and the 95% CIs of the 7 additive components of the SAGP model on 100 equispaced locations on the support of the data. Panel (b) shows the posterior means and the 95% CIs of the sole component in layer 1 (red), of the components belonging to layer 1 and 2 (green) and of the complete model, including components from layer 1, 2 and 3. Panel (c) provides the predictive mean and the corresponding 95% prediction intervals.



5.2 Temperature Data

Non-stationary datasets occur in various scenarios like spatial statistics, geology and time series. There are multiple approaches to modeling spatial datasets with non-stationary features besides covariance kernel methods [Paciorek and Schervish, 2004]. Deformation methods [Sampson and Guttorp, 1992], dimension expansion methods [Borner et al., 2012] and locally stationary modelings [Dahlhaus, 2012] are all state-of-art methods and well studied. In this section we will compare the performance of the SAGP model to the full GP (also known under the name kriging in spatial statistics) and BART. The SGP can be viewed as a special case for our SAGP and we compare the SAGP model with GP and BART, which appear to have the best performance in the simulation study (see Section 4).

The dataset we analyzed here is the US precipitation and temperature (1895-1997) dataset well analyzed in spatial statistics literature. This dataset contains average daily maximum temperature recorded in units of degree centigrade by weather stations in the United States from 1895 through 1997. Paciorek and Schervish [2006] analyzed its non-stationary features using precipitation data. We apply the SAGP model to capture the non-stationarity evident in the spatial data. We discard all missing observations contained in the data and consider the maximum average temperature of an area in Colorado (Longitude: -109.483 to -101.02; latitude: 36.55 to 41.45) in summer of year 1997. There are 247 input locations in $X \subset \mathbb{R}^2$ containing non-missing records during this period of time and for each location we record the maximum average temperature data in centigrade degree as response y .

For Gaussian process regression (kriging) we use MLE estimation with *Matern*(5/2) kernel via the *DiceKriging* package [Olivier et al., 2012]. The result shows reasonable predictions at the observed locations. However, the prediction comes with high predictive variance in locations other than those observed locations, especially when the predictive location is outside the range of observed datasets and close to the boundary of the input domain. For BART we use the *BayesTree* package with its default settings [Chipman et al., 2010]. We can see from its result that the predictive mean of BART shows its characteristic grid-like shape. In addition it also fails to delineate the shapes of the modal peaks, which has been captured by GP regression. In addition, neither BART nor GP regression provide informative uncertainty quantification. In BART model, the standard deviation does not seem to have any continuity.

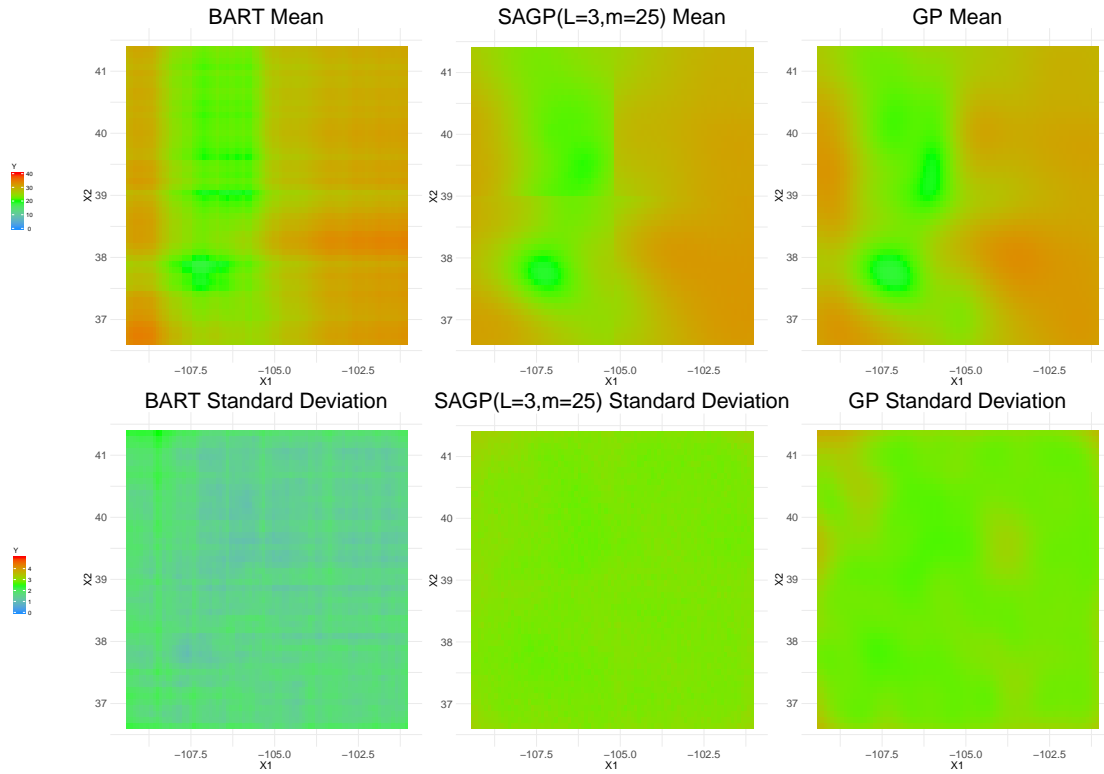
For applying of SAGP, we perform 10-fold cross-validation to determine the most appropriate parameter values L, m as shown in Figure 4(b). Based on the MSE evaluation as well as the limitation of the amount of data, we choose the combination of $L = 3, m = 25$ to fit SAGP. Here we also calibrate the α, β of the noise prior in SAGP and the noise estimate in BART according to MLE of noise variance from GP.

This dataset provides us an example where the data is limited, which is actually a disadvantage for SAGP since the sparsification does not cut down the computational cost significantly yet some information is lost in the procedure. Nonetheless, the SAGP method does capture the major trends and even some of the extremal temperatures close to 40 centigrade degrees. It also exhibits the major modes in the dataset. We can see from the plot of predictive mean and standard deviation that SAGP does capture the trend in both mean and preserve relatively low uncertainty. In this case where there is not enough data to go to more complicated models, SAGP has some clear borders close to the RP boundaries. However, it still performs surprisingly well and competitive to the performance of the full GP.

Figure 6: The original max temperature dataset for Colorado in 1997 summer. The horizontal X_1 axis is longitude; the vertical X_2 axis is latitude; the Y value is the observed values of maximal temperature in degree.



Figure 7: The typical raster plot for predictive means and standard deviations of Gaussian Process regression (Universal kriging with Gaussian kernel and MLE nuggets)/BART(number of trees $m = 200$)/SAGP($L = 4, m = 10$) for max temperature dataset and evaluation on a fine meshed grid (generated by steplong 0.1) on the original input domain $X = [0, 1]^2$. The axes are the same as in Figure 6.



6 Conclusion

The SAGP model effectively borrows ideas from both sparsification and localization. There are various possible extensions of the proposed SAGP model which are not pursued in the current paper. We can ask questions concerning its sparsification scheme or its partition scheme separately but we intend not to provide an exhaustive investigation here.

Other than this advantage of capturing nonstationarity, since independent sparse Gaussian process (SGP) regression model are fitted for each local component in the same layer of the RP scheme, it is readily seen that our model is parallelizable for efficient computation. Both the GP fitting with latent variable approximation approach [Chen et al., 2013] and the tree-like Bayesian model fitting approach [Pratola et al., 2014] can be adapted to parallel computing algorithms, therefore our model and approach are extensible to larger scale datasets. This point is also supported by our simulation and real-data results in the performance evaluation section of the paper.

As a Bayesian model, it is a question whether such a model always converges when fitted by MCMC. In the implementation of our model, the acceptance rate of the MCMC is controlled by using an adaptive choice of the bandwidth of the proposal distribution. In general we found the SAGP model mixed well and reasonably fast based on its trace-plot and associated diagnostics. In the case of 1-dimensional input domain, we checked the mixing diagnostics statistics based on the MCMC samples as suggested in Gelman et al. [2013]. This check confirmed that our model mixes well in the $d = 1$ case. But it is not known at the time that such diagnostics will generalize into higher dimensional data. In a higher dimensional input domain like the precipitation dataset, we looked at both the acceptance rate and the corresponding diagnostic for each (one dimensional) coordinate of the parameters in the model and the trace-plots to confirm that the model appears to converge. However, even if all these post hoc diagnostics do not flag a warning, it is still possible that in higher dimensions the Bayesian model might have difficulty converging. But this criticism also applies to the diagnostic of all high dimensional Bayesian MCMC results [Gelman et al., 2013].

With the proposed RP scheme, the SAGP model is way more flexible in terms of admitting various partition schemes, this power is gained from adopting a fully Bayesian framework additive modeling with back-fitting. This Bayesian modeling with back-fitting scheme elegantly solves the problem of specification of inter-component covariance discussed in Nguyen-Tuong et al. [2009] and Lee et al. [2017]. In higher dimensions, SAGP can be easily generalized without much increase of computational cost while multi-scale regression seems incapable of handling higher dimensional datasets without a delicate design of partition schemes and inter-block kernels. In the homogeneous case, our RP partition scheme is similar to Bui and Turner [2014] and Lee et al. [2017]; in heterogeneous tree in higher dimensions, our RP partition scheme is more flexible. For example, we can use binary partitioning in the first dimension but ternary partitioning in the second dimension.

How we specify the priors may also be affected by the form of covariance kernel. It is natural to assume $\mathbf{x} \in B_{\mu_j}(\sigma_j)$ because we do not want to extrapolate with \mathbf{f}_j outside $B^{(j)}$. But it is reasonable to use compactly support kernels that are supported on $B_{\mu_j}(\sigma_j)$ like Epanechnikov kernel or kernels with certain degree of regularity like Matérn kernel family according to specific applications [Rasmussen and Williams, 2006]. The choice of Gaussian kernel in (4) is simply out of convenience. Furthermore, if we want to extrapolate with component mean function \mathbf{f}_j under the situation when there are insufficient data, we may either use a coarser RP scheme or choose kernels that decay fast outside the components of the RP scheme. These choices of different kernels may greatly affect the performance and hyper-parameter specification and is out of the scope of the current paper but of future interest.

The main contribution in this work is to incorporate both the idea of sparsification via pseudo-inputs and the RP scheme to ensure a balance between flexibility and efficiency. It is also capable of handling non-stationary data as shown; and the trade-off between partition scheme and extent of sparsification in terms of number of pseudo-inputs allows for easy tuning of the SAGP model.

A MCMC Algorithm for SAGP Model Fitting (Algorithm 3)

Algorithm 3 MCMC algorithm for SAGP model.

Input : RP partition scheme consisting of N components, Number of pseudo-inputs for each component m_j , Hyper-parameters for the prior of parameters, Observed dataset $\{\mathcal{X}, \mathbf{y}\}$.

Output : Posterior samples for parameters, $\bar{\mathcal{X}}^{(j)}, \bar{\mathbf{f}}_j$, Predictive posterior samples for $\mathbf{y}_*, \mathbf{f}_j, \mathbf{y}$.

```

1 Initialization of the parameter values
2 while not converged do
3   Sample  $\bar{\mathcal{X}}^{(j)}, j = 1, \dots, N$  as in Algorithm 2.
4   for  $j$  in  $1 : N$  do
5      $\mathbf{r}_j \leftarrow \mathbf{y} - \sum_{l \neq j} \mathbf{K}_{nm_l}^{(l)} \left( \mathbf{K}_{m_l}^{(l)} \right)^{-1} \bar{\mathbf{f}}_l$ 
6      $\bar{\mathbf{f}}_j \leftarrow N_{m_j}(\text{Mean}_j, \text{Var}_j)$  as in (22)
7      $\eta_{j,\text{new}} \leftarrow \text{Uniform}(\eta_j \pm \text{bandwidth})$ 
8      $\alpha \leftarrow \min(1, C \cdot \text{Model Likelihood}(\eta_{j,\text{new}}) / C \cdot \text{Model Likelihood}(\eta_j))$ 
9     if  $\text{Uniform}(0, 1) \leq \alpha$  then
10       $\eta_j \leftarrow \eta_{j,\text{new}}$ 
11    end
12    // For every burn-in steps/20 steps, we adjust bandwidth.
13    if Acceptance rate of  $\eta_j \notin (0.39, 0.49]$  then
14      Band width for proposing  $\eta_j \leftarrow \text{Acceptance rate of } \eta_j / 0.44$ 
15    end
16   $\sigma_\epsilon^2 \leftarrow \text{InverseGamma}(\alpha_\epsilon + \frac{n}{2}, \beta_\epsilon + \frac{1}{2}(\mathbf{y} - \hat{\mathbf{y}})^T(\mathbf{y} - \hat{\mathbf{y}}))$ 
17 end
```

B Detailed Derivation of Posterior Distribution in Section 3.2.5

To clarify our derivations, we first stated following simple lemma that will be used, which can be derived from Woodbury identity [Horn and Johnson, 1990] or a direct verification [Rasmussen and Williams, 2006].

Lemma 1 For a joint Gaussian distribution $\mathbf{a} \in \mathbb{R}^n, \mathbf{b} \in \mathbb{R}^m$ if

$$\begin{pmatrix} \mathbf{a} \\ \mathbf{b} \end{pmatrix} \propto N_{n+m} \left(\begin{pmatrix} \boldsymbol{\mu}_a \\ \boldsymbol{\mu}_b \end{pmatrix}, \begin{pmatrix} C_{aa} & C_{ab} \\ C_{ba} & C_{bb} \end{pmatrix} \right) \quad (24)$$

then its conditional distribution is:

$$\mathbf{a} \mid \mathbf{b} \sim N_n \left(\boldsymbol{\mu}_a + C_{ab} (C_{bb})^{-1} (\mathbf{b} - \boldsymbol{\mu}_b), C_{aa} - C_{ab} (C_{bb})^{-1} C_{ba} \right) \quad (25)$$

In particular, for $f_l = f(\mathbf{x}_l), \bar{\mathbf{f}}_j = (\bar{f}_j(\bar{\mathbf{x}}_1), \dots, \bar{f}_j(\bar{\mathbf{x}}_{m_j}))^T$ and covariance kernel function $K = K^{(j)}, K_{ll}^{(j)} = K^{(j)}(\mathbf{x}_l, \mathbf{x}_l)$ if

$$\begin{pmatrix} f_l \\ \bar{\mathbf{f}}_j \end{pmatrix} \mid \bar{\mathcal{X}}^{(j)}, \mathbf{x}_l \propto N_{1+m_j} \left(\begin{pmatrix} 0 \\ \mathbf{0}_{m_j} \end{pmatrix}, \begin{pmatrix} K_{ll}^{(j)} & \mathbf{k}_l^{(j)T} \\ \mathbf{k}_l^{(j)} & \mathbf{K}_{m_j}^{(j)} \end{pmatrix} \right) \quad (26)$$

then its conditional distribution is:

$$f_l \mid \bar{\mathbf{f}}_j, \bar{\mathcal{X}}^{(j)}, \mathbf{x}_l \sim N_1 \left(\mathbf{k}_l^{(j)T} \left(\mathbf{K}_{m_j}^{(j)} \right)^{-1} \bar{\mathbf{f}}_j, K_{ll}^{(j)} - \mathbf{k}_l^{(j)T} \left(\mathbf{K}_{m_j}^{(j)} \right)^{-1} \mathbf{k}_l^{(j)} \right) \quad (27)$$

We assume a Gaussian prior on the pseudo-targets as in (3.2.2).

$$P(\bar{\mathbf{f}}_j \mid \bar{\mathcal{X}}^{(j)}) \sim N_{m_j} \left(\bar{\mathbf{f}}_j \mid \mathbf{0}_{m_j}, \mathbf{K}_{m_j}^{(j)} \right) \quad (28)$$

and then use Bayesian rule on the parameter $\bar{\mathbf{f}}_j$, recalling that (3) determines the form of mean and variance of the Gaussian distribution $P(\mathbf{y} \mid \bar{\mathbf{f}}_1, \dots, \bar{\mathbf{f}}_N, \bar{\mathcal{X}}^{(1)}, \dots, \bar{\mathcal{X}}^{(N)}, \mathcal{X}, \boldsymbol{\kappa})$.

$$\begin{aligned} & P(\bar{\mathbf{f}}_j \mid \mathbf{y}, \mathcal{X}, \bar{\mathbf{f}}_1, \dots, \bar{\mathbf{f}}_N, \bar{\mathcal{X}}^{(1)}, \dots, \bar{\mathcal{X}}^{(N)}, \boldsymbol{\kappa}) \\ & \propto P(\mathbf{y} \mid \bar{\mathbf{f}}_1, \dots, \bar{\mathbf{f}}_N, \bar{\mathcal{X}}^{(1)}, \dots, \bar{\mathcal{X}}^{(N)}, \boldsymbol{\kappa}) \times \\ & P(\bar{\mathbf{f}}_j \mid \{\mathbf{x}\}_n, \bar{\mathbf{f}}_1, \dots, \bar{\mathbf{f}}_{j-1}, \bar{\mathbf{f}}_{j+1}, \dots, \bar{\mathbf{f}}_N, \bar{\mathcal{X}}^{(1)}, \dots, \bar{\mathcal{X}}^{(N)}, \boldsymbol{\kappa}) \end{aligned} \quad (29)$$

$$\begin{aligned} & = N_n \left(\mathbf{y} - \sum_{l \neq j} \mathbf{K}_{nm_l}^{(l)} \left(\mathbf{K}_{m_l}^{(l)} \right)^{-1} \bar{\mathbf{f}}_l \mid \mathbf{K}_{nm_j}^{(j)} \left(\mathbf{K}_{m_j}^{(j)} \right)^{-1} \bar{\mathbf{f}}_j, \boldsymbol{\Lambda}_n^{(j)} + \sigma_\epsilon^2 \mathbf{I}_n \right) \times \\ & N_{m_j} \left(\bar{\mathbf{f}}_j \mid \mathbf{0}_{m_j}, \mathbf{K}_{m_j}^{(j)} \right) \end{aligned} \quad (30)$$

We can derive the posterior using the normal normal conjugacy:

$$\begin{aligned} & P(\bar{\mathbf{f}}_j \mid \mathbf{y}, \mathcal{X}, \bar{\mathbf{f}}_1, \dots, \bar{\mathbf{f}}_{j-1}, \bar{\mathbf{f}}_{j+1}, \dots, \bar{\mathbf{f}}_N, \bar{\mathcal{X}}^{(1)}, \dots, \bar{\mathcal{X}}^{(N)}, \boldsymbol{\kappa}) \\ & \propto \frac{1}{\sqrt{|2\pi (\boldsymbol{\Lambda}_n^{(j)} + \sigma_\epsilon^2 \mathbf{I}_n)|}} \exp \left\{ -\frac{1}{2} \left[\mathbf{y} - \sum_{l=1}^N \mathbf{K}_{nm_l}^{(l)} \left(\mathbf{K}_{m_l}^{(l)} \right)^{-1} \bar{\mathbf{f}}_l \right]^T \left(\boldsymbol{\Lambda}_n^{(j)} + \sigma_\epsilon^2 \mathbf{I}_n \right)^{-1} \times \right. \\ & \left. \left[\mathbf{y} - \sum_{l=1}^N \mathbf{K}_{nm_l}^{(l)} \left(\mathbf{K}_{m_l}^{(l)} \right)^{-1} \bar{\mathbf{f}}_l \right] \right\} \times \\ & \frac{1}{\sqrt{|2\pi \mathbf{K}_{m_j}^{(j)}|}} \exp \left\{ -\frac{1}{2} \bar{\mathbf{f}}_j^T \mathbf{K}_{m_j}^{(j)-1} \bar{\mathbf{f}}_j \right\} \end{aligned} \quad (31)$$

We complete the squares inside the exponent,

$$\begin{aligned} & \propto \exp \left\{ -\frac{1}{2} \bar{\mathbf{f}}_j^T \left(\mathbf{K}_{m_j}^{(j)-1} + \left[\left(\mathbf{K}_{m_j}^{(j)} \right)^{-1} \mathbf{K}_{m_j n}^{(j)} \left(\boldsymbol{\Lambda}_n^{(j)} + \sigma_\epsilon^2 \mathbf{I}_n \right)^{-1} \mathbf{K}_{nm_j}^{(j)} \left(\mathbf{K}_{m_j}^{(j)} \right)^{-1} \right] \right) \bar{\mathbf{f}}_j \right. \\ & \left. - \bar{\mathbf{f}}_j^T \left(\boldsymbol{\Lambda}_n^{(j)} + \sigma_\epsilon^2 \mathbf{I}_n \right)^{-1} \mathbf{K}_{nm_j}^{(j)} \left(\mathbf{K}_{m_j}^{(j)} \right)^{-1} \bar{\mathbf{f}}_j + \text{proportionally constant terms} \right\} \end{aligned} \quad (32)$$

After completing square we can obtain the mean and variance of the j -th component:

$$\begin{aligned} & \text{Mean}_j = \left(\left(\mathbf{K}_{m_j}^{(j)} \right)^{-1} + \left[\left(\mathbf{K}_{m_j}^{(j)} \right)^{-1} \mathbf{K}_{m_j n}^{(j)} \left(\boldsymbol{\Lambda}_n^{(j)} + \sigma_\epsilon^2 \mathbf{I}_n \right)^{-1} \mathbf{K}_{nm_j}^{(j)} \left(\mathbf{K}_{m_j}^{(j)} \right)^{-1} \right] \right) \times \\ & \left(\left(\mathbf{y} - \sum_{l \neq j} \mathbf{K}_{nm_l}^{(l)} \left(\mathbf{K}_{m_l}^{(l)} \right)^{-1} \bar{\mathbf{f}}_l \right)^T \left(\boldsymbol{\Lambda}_n^{(j)} + \sigma_\epsilon^2 \mathbf{I}_n \right)^{-1} \mathbf{K}_{nm_j}^{(j)} \left(\mathbf{K}_{m_j}^{(j)} \right)^{-1} \right)^T \\ & = \mathbf{K}_{m_j}^{(j)} \mathbf{Q}_{m_j}^{(j)-1} \mathbf{K}_{m_j n}^{(j)} \left(\boldsymbol{\Lambda}_n^{(j)} + \sigma_\epsilon^2 \mathbf{I}_n \right)^{-1} \left(\mathbf{y} - \sum_{l \neq j} \mathbf{K}_{nm_l}^{(l)} \left(\mathbf{K}_{m_l}^{(l)} \right)^{-1} \bar{\mathbf{f}}_l \right) \end{aligned} \quad (33)$$

By Woodbury identity, we know that for $\mathbf{Q}_{m_j}^{(j)} = \mathbf{K}_{m_j}^{(j)} + \mathbf{K}_{m_j n}^{(j)} \left(\boldsymbol{\Lambda}_n^{(j)} + \sigma_\epsilon^2 \mathbf{I}_n \right)^{-1} \mathbf{K}_{nm_j}^{(j)}$ we can write its inverse as

$$\mathbf{Q}_{m_j}^{(j)-1} = \left\{ \mathbf{K}_{m_j}^{(j)-1} - \mathbf{K}_{m_j}^{(j)-1} \mathbf{K}_{m_j n}^{(j)} \left[\left(\boldsymbol{\Lambda}_n^{(j)} + \sigma_\epsilon^2 \mathbf{I}_n \right) + \mathbf{K}_{nm_j}^{(j)} \mathbf{K}_{m_j}^{(j)-1} \mathbf{K}_{m_j n}^{(j)} \right]^{-1} \mathbf{K}_{nm_j}^{(j)} \mathbf{K}_{m_j}^{(j)-1} \right\}$$

Using this $m_j \times m_j$ matrix \mathbf{Q}_{m_j} , we can write down the covariance matrix \mathbf{Var}_j :

$$\mathbf{Var}_j = \left(\left(\mathbf{K}_{m_j}^{(j)} \right)^{-1} + \left[\left(\mathbf{K}_{m_j}^{(j)} \right)^{-1} \mathbf{K}_{m_j n}^{(j)} \left(\mathbf{\Lambda}_n^{(j)} + \sigma_\epsilon^2 \mathbf{I}_n \right)^{-1} \mathbf{K}_{n m_j}^{(j)} \left(\mathbf{K}_{m_j}^{(j)} \right)^{-1} \right] \right)^{-1} \quad (34)$$

$$\begin{aligned} &= \mathbf{K}_{m_j}^{(j)} - \mathbf{K}_{m_j}^{(j)} \left[\left(\mathbf{K}_{m_j}^{(j)} \right)^{-1} \mathbf{K}_{m_j n}^{(j)} \right] \times \\ &\quad \left[\left(\mathbf{\Lambda}_n^{(j)} + \sigma_\epsilon^2 \mathbf{I}_n \right) + \mathbf{K}_{n m_j}^{(j)} \left(\mathbf{K}_{m_j}^{(j)} \right)^{-1} \mathbf{K}_{m_j}^{(j)} \left(\mathbf{K}_{m_j}^{(j)} \right)^{-1} \mathbf{K}_{m_j n}^{(j)} \right]^{-1} \times \\ &\quad \mathbf{K}_{n m_j}^{(j)} \left(\mathbf{K}_{m_j}^{(j)} \right)^{-1} \mathbf{K}_{m_j}^{(j)} \end{aligned} \quad (35)$$

$$\begin{aligned} &= \mathbf{K}_{m_j}^{(j)} - \mathbf{K}_{m_j n}^{(j)} \left[\left(\mathbf{\Lambda}_n^{(j)} + \sigma_\epsilon^2 \mathbf{I}_n \right) + \mathbf{K}_{n m_j}^{(j)} \left(\mathbf{K}_{m_j}^{(j)} \right)^{-1} \mathbf{K}_{m_j}^{(j)} \right]^{-1} \mathbf{K}_{n m_j}^{(j)} \\ &= \mathbf{K}_{m_j}^{(j)} \left\{ \left(\mathbf{K}_{m_j}^{(j)} \right)^{-1} - \right. \\ &\quad \left. \left(\mathbf{K}_{m_j}^{(j)} \right)^{-1} \mathbf{K}_{m_j n}^{(j)} \left[\left(\mathbf{\Lambda}_n^{(j)} + \sigma_\epsilon^2 \mathbf{I}_n \right) + \mathbf{K}_{n m_j}^{(j)} \left(\mathbf{K}_{m_j}^{(j)} \right)^{-1} \mathbf{K}_{m_j}^{(j)} \right]^{-1} \left(\mathbf{K}_{m_j}^{(j)} \right)^{-1} \right\} \mathbf{K}_{n m_j}^{(j)} \end{aligned} \quad (36)$$

$$= \mathbf{K}_{m_j}^{(j)} \mathbf{Q}_{m_j}^{(j)-1} \mathbf{K}_{m_j}^{(j)} \quad (37)$$

Note that although we do need to invert an $n \times n$ matrix $\mathbf{\Lambda}_n^{(j)} + \sigma_\epsilon^2 \mathbf{I}_n$, it is a diagonal matrix and hence easy to invert as claimed before.

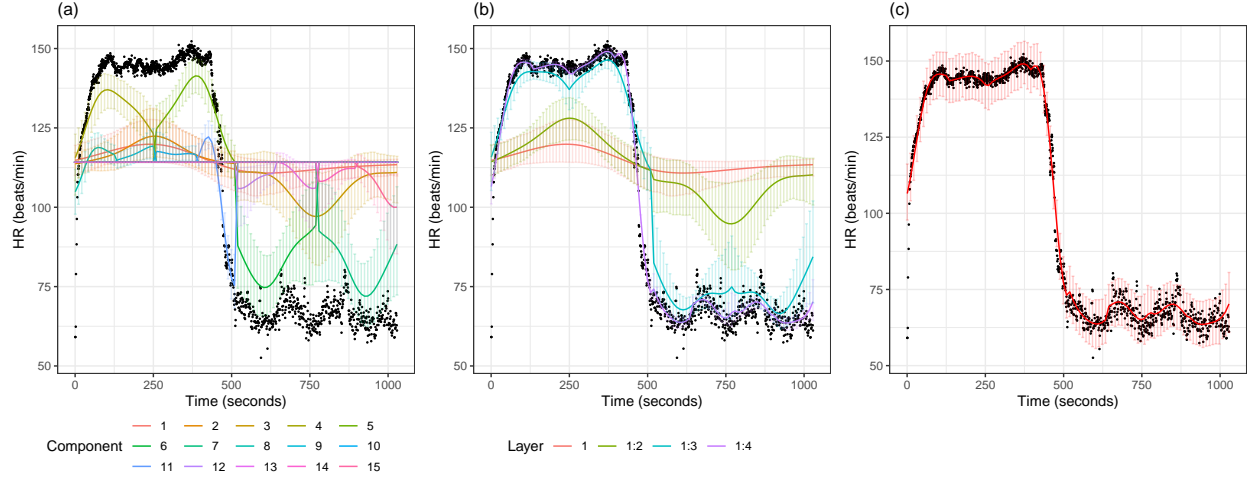
C Proof of Proposition 1

We first calculate the total number of components in the SAGP models when the input-domain is $[0, 1]^d$. For each dimension $i = 1, 2, \dots, d$, if we b_i -ary subdivide the $[0, 1]$ interval, then there are $|\mathcal{L}_\ell| = \prod_{i=1}^d b_i^{\ell-1}$ individual components in form of $B_{\mu_j}(\sigma_j)$ in the ℓ -th layer of the RP scheme for $\ell = 1, 2, \dots, L$.

For each component B in the ℓ -th layer, the number of observations fitted to the component B is $n_B = n$. Then we fit a SGP model with m pseudo-inputs, whose complexity is $\mathcal{O}(n_B \cdot m^2)$. Then for the ℓ -th layer the total complexity is $\mathcal{O}(\sum_{B \in \mathcal{L}_\ell} n_B \cdot m^2) = \mathcal{O}(|\mathcal{L}_\ell| \cdot n \cdot m^2)$. Therefore for the ℓ -th layer the complexity is $\mathcal{O}(|\mathcal{L}_\ell| \cdot n \cdot m^2)$. Therefore we can compute the total complexity of the model as $\mathcal{O}(\sum_{\ell=1}^L |\mathcal{L}_\ell| \cdot n \cdot m^2) = \mathcal{O}\left(\sum_{\ell=1}^L \prod_{i=1}^d b_i^{\ell-1} \cdot n \cdot m^2\right)$.

D Heart Rate Dataset analyzed by SAGP model fitted with $m = 5$ and $L = 4$ (Figure 8)

Figure 8: The panels show the observed HR values over time as black dots and results about the fit of the SAGP model with $m = 5$ and $L = 4$. Panel (a) shows the posterior means and the 95% CIs of the 15 additive components of the SAGP model on 100 equispaced locations on the support of the data. Panel (b) shows the posterior means and the 95% CIs of the sole component in layer 1 (red), of the components belonging to layer 1 and 2 (green), of the components belonging to layer 1, 2, 3 and of the complete model, including components from layer 1, 2, 3 and 4. Panel (c) provides the predictive mean and the corresponding 95% prediction intervals.



References

- Amy Racine-Poon & Adrian F. M. Smith Alan E. Gelfand, Susan E. Hills. Illustration of bayesian inference in normal data models using gibbs sampling. *Journal of the American Statistical Association*, pages 972–985, 1990.
- Vânia G Almeida and Ian T Nabney. Early warnings of heart rate deterioration. In *Engineering in Medicine and Biology Society (EMBC), 2016 IEEE 38th Annual International Conference of the*, pages 940–943. IEEE, 2016.
- Anjishnu Banerjee, David B. Dunson, and Surya T. Tokdar. Efficient gaussian process regression for large datasets. *Biometrika*, 100.1:75–89, 2012.
- Jon Louis. Bentley. Multidimensional binary search trees used for associative searching. *Communications of the ACM*, 18.9:509–517., 1975.
- Luke Bornn, Gavin Shaddick, and James V. Zidek. Modeling nonstationary processes through dimension expansion. *Journal of the American Statistical Association*, 107.497:281–289, 2012.
- Leo Breiman. *Classification and regression trees*. Wadsworth, 1984.
- Thang D. Bui and Richard E. Turner. Tree-structured gaussian process approximations. In *Advances in Neural Information Processing Systems*, 2014.
- Jie Chen et al. Parallel gaussian process regression with low-rank covariance matrix approximations. *arXiv preprint arXiv:1305.5826*, 2013.
- Hugh A. Chipman, Edward I. George, and Robert E. McCulloch. Bayesian cart model search. *Journal of the American Statistical Association*, 93.443:935–948, 1998.
- Hugh A. Chipman, Edward I. George, and Robert E. McCulloch. Bart: Bayesian additive regression trees. *The Annals of Applied Statistics*, 4.1:266–298, 2010.
- Hugh A Chipman et al. High-dimensional nonparametric monotone function estimation using bart. *arXiv preprint arXiv:1612.01619*, 2016.
- Glen Wright Colopy, Marco AF Pimentel, Stephen J Roberts, and David A Clifton. Bayesian gaussian processes for identifying the deteriorating patient. In *Engineering in Medicine and Biology Society (EMBC), 2016 IEEE 38th Annual International Conference of the*, pages 5311–5314. IEEE, 2016.
- Rainer Dahlhaus. *Handbook of statistics, Locally stationary processes*, pages 351–413. Elsevier, 2012.

- Andreas Damianou and Neil Lawrence. Deep gaussian processes. *Artificial Intelligence and Statistics*, 2013.
- David GT Denison, Bani K Mallick, and Adrian FM Smith. A bayesian cart algorithm. *Biometrika*, 85(2):363–377, 1998.
- Emily Fox and David B. Dunson. Multiresolution gaussian processes. *Advances in Neural Information Processing Systems*, 2012.
- Andrew Gelman et al. *Bayesian data analysis*. Chapman and Hall/CRC, 2013.
- Tilmann Gneiting and Adrian E Raftery. Strictly proper scoring rules, prediction, and estimation. *Journal of the American Statistical Association*, 102(477):359–378, 2007.
- Robert B. Gramacy and Daniel W. Apley. Local gaussian process approximation for large computer experiments. *Journal of Computational and Graphical Statistics*, 24.2:561–578, 2015.
- Trevor Hastie and Robert Tibshirani. Bayesian backfitting (with comments and a rejoinder by the authors. *Statistical Science*, 15.3:196–223, 2000.
- Trevor J. Hastie and R.J. Tibshirani. *Generalized additive models*. Chapman and Hall/CRC, 1990.
- Roger A. Horn and Charles R. Johnson. *Matrix analysis*. Cambridge university press, 1990.
- Matthias Katzfuss. A multi-resolution approximation for massive spatial datasets. *Journal of the American Statistical Association*, 112(517):201–214, 2017.
- Matthias Katzfuss and Wenlong Gong. A class of multi-resolution approximations for large spatial datasets. *arXiv preprint arXiv:1710.08976*, 2017.
- Cari G Kaufman, Mark J. Schervish, and Douglas W. Nychka. Covariance tapering for likelihood-based estimation in large spatial data sets. *Journal of the American Statistical Association*, 103.484:1545–1555, 2008.
- Neil D. Lawrence, Ralf Herbrich, and Matthias Seeger. Fast sparse gaussian process methods: The informative vector machine. In *Advances in neural information processing systems*, 2003.
- Byung-Jun Lee, Jongmin Lee, and Kee-Eung Kim. Hierarchically-partitioned gaussian process approximation. In *Artificial Intelligence and Statistics*, 2017.
- Haitao Liu et al. When gaussian process meets big data: A review of scalable gps. *arXiv preprint arXiv:1807.01065*, 2018.
- Duy Nguyen-Tuong, Matthias Seeger, and Jan Peters. Model learning with local gaussian process regression. *Advanced Robotics*, 23.15:2015–2034, 2009.
- Roustant Olivier, David Ginsbourger, and Yves Deville. Dicekriging, diceoptim: Two r packages for the analysis of computer experiments by kriging-based metamodeling and optimization. *Journal of Statistical Software*, 2012.
- Christopher J Paciorek and Mark J. Schervish. Nonstationary covariance functions for gaussian process regression. *Advances in neural information processing systems*, 2004.
- Christopher J Paciorek and Mark J. Schervish. Spatial modelling using a new class of nonstationary covariance functions. *Environmetrics: The official journal of the International Environmetrics Society*, 17.5:483–506, 2006.
- Chiwoo Park and Daniel Apley. Patchwork kriging for large-scale gaussian process regression. *The Journal of Machine Learning Research*, 19.1:269–311, 2018.
- Chiwoo Park and Jianhua Z. Huang. Efficient computation of gaussian process regression for large spatial data sets by patching local gaussian processes. *Journal of Machine Learning Research*, 17:1–29, 2016.
- Matthew Pratola et al. Heteroscedastic bart using multiplicative regression trees. *arXiv:1709.07542*, pages 1–33, 2018.
- Matthew T. Pratola. Efficient metropolis–hastings proposal mechanisms for bayesian regression tree models. *Bayesian analysis*, 11.3:885–911, 2016.
- Matthew T Pratola, Hugh A Chipman, James R Gattiker, David M Higdon, Robert McCulloch, and William N Rust. Parallel bayesian additive regression trees. *Journal of Computational and Graphical Statistics*, 23(3):830–852, 2014.
- Matthew T Pratola, C Devon Lin, and Peter F Craigmile. Optimal design emulators: A point process approach. *arXiv preprint arXiv:1804.02089*, 2019.
- Joaquin Quinonero-Candela and Carl Edward Rasmussen. A unifying view of sparse approximate gaussian process regression. *Journal of Machine Learning Research*, 6:1939–1959, 2005.
- Carl Edward Rasmussen and Christopher KI Williams. *Gaussian process for machine learning*. MIT press, 2006.
- Christian Robert and George Casella. A short history of markov chain monte carlo: Subjective recollections from incomplete data. *Statistical Science*, pages 102–115, 2011.

- Olivier Roustant, David Ginsbourger, and Yves Deville. Dicekriging, diceoptim: Two r packages for the analysis of computer experiments by kriging-based metamodeling and optimization. 2012.
- Daniel M. Roy and Yee Whye Teh. The mondrian process. In *NIPS*, 2008.
- Paul D. Sampson and Peter Guttorp. Nonparametric estimation of nonstationary spatial covariance structure. *Journal of the American Statistical Association*, 87.417:108–119, 1992.
- Edward Snelson and Zoubin Ghahramani. Sparse gaussian processes using pseudo-inputs. In *Advances in neural information processing systems*, 2006.
- Edward Snelson and Zoubin Ghahramani. Local and global sparse gaussian process approximations. In *Artificial Intelligence and Statistics*, 2007.
- James Andrew Storer. *An introduction to data structures and algorithms*. Springer Science & Business Media, 2012.
- Michali Titsias. Variational learning of inducing variables in sparse gaussian processes. *Artificial Intelligence and Statistics*, 2009a.
- Michalis Titsias. Variational model selection for sparse gaussian process regression. Technical report, University of Manchester, UK., 2009b.
- Maria S Zakynthinaki. Modelling heart rate kinetics. *PloS one*, 10(4):e0118263, 2015.